DOI:10.14753/SE.2025.3206

SEMMELWEIS EGYETEM

DOKTORI ISKOLA

Ph.D. értekezések

3206.

ZICHÓ KRISZTIÁN

Neuromorfológia és sejtbiológia

című program

Programvezető: Dr. Alpár Alán, egyetemi tanár, az MTA doktora

Témavezető: Dr. Nyiri Gábor, tudományos főmunkatárs

DOI:10.14753/SE.2025.3206

THE BRAINSTEM CONTROL OF LATERAL HABENULA

PhD thesis

Krisztián Zichó

Semmelweis University Doctoral School
Szentágothai János Neurosciences Division

Supervisor: Gábor Nyiri, D.Sc.

Official reviewers: Gergely Zachar, PhD

Attila Tóth, D.Sc.

Head of the Complex Examination Committee:

Alán Alpár, D.Sc.

Members of the Complex Examination Committee:

Árpád Dobolyi, D.Sc.

Ádám Dénes, D.Sc.

Budapest

2025

DOI:10.14753/SE.2025.3206

Table of Contents

1. Introduction
   1.1. Emotional valence and mood regulation
   1.2. Mood-related disorder: depression
   1.3. General neuroanatomical background of the regulation of emotional valence
   1.4. Ventral tegmental area: The neuronal hub for reward processing
   1.5. Lateral habenula: The neuronal hub for processing emotional balance
   1.6. The role of lateral habenula in depression
   1.7. Pontine brainstem role in regulating emotions
2. Objectives
   2.1. Excitatory Innervation to the LHb from the Brainstem
   2.2. Inhibitory Innervation to the LHb from the Brainstem
3. Methods
   3.1. Ethical consideration
   3.2. Mice and rats
   3.3. Macaque monkey
   3.4. Human samples
   3.5. Stereotaxic surgeries for viral gene transfer, retrograde tracing, and optic fiber implantation
   3.6. Mono-transsynaptic rabies tracing
   3.7. Perfusion and sectioning
   3.8. Antibodies
   3.9. Fluorescent immunohistochemistry, epifluorescent and laser-scanning confocal microscopy for counting cells and synaptic contacts
   3.10. Stereological measurement
   3.11. Immunoperoxidase staining and imaging for rat, macaque, and human brain slices
   3.12. Real-time and conditioned place preference (RTPP, CPP) or aversion (RTPA, CPA) tests
   3.13. Aversive operant conditioning test
   3.14. Operant self-stimulation test
   3.15. Cued fear conditioning test
   3.16. Contextual fear conditioning test

3.17. Analysis and statistics for behavioral experiments

4. Results
4.1. Excitatory innervation to the LHb from the Brainstem
4.1.1. vGluT2 neurons are the largest population of projection cells in the MRR that innervates aversive and memory formation-related nuclei
4.1.2. MRR vGluT2 neurons innervate aversive and memory formation-related nuclei
4.1.3. MRR vGluT2 neurons receive inputs from negative experience processing brain regions
4.1.4. Stimulation of MRR vGluT2 neurons causes strongly aversive behavior
4.1.5. MRR vGluT2 neurons are necessary for fear memory formation
4.2. Inhibitory innervation to the LHb from the Brainstem
4.2.1. A novel LHb-innervating pontine GABAergic nucleus: the SVTg
4.2.2. Stimulation of SVTg induces positive valence and reward-seeking behavior
4.2.3. Activity of SVTg is required for a balanced assessment of valence
4.2.4. SVTg neurons receive inputs from valence and salience-processing brain areas
4.2.5. Typical molecular features of SVTg neurons
4.2.6. SVTg in rodents, primates, and the human brain
5. Discussion
5.1. Brainstem control of emotional balance
5.2. The role of MRR vGluT2-positive neurons in processing negative experiences
5.3. The role of SVTg neurons in processing positive experiences
5.4. Interactions between MRR vGluT2 and SVTg GABAergic neurons
5.5. Future therapeutic potential of MRR and SVTg
6. Conclusions
7. Summary
8. References
9. Bibliography of the candidate's publications
10. Acknowledgements

List of Abbreviations

4V: fourth ventricle
AAV: adeno-associated virus
aPVT: anterior paraventricular thalamic nucleus
ArchT: archaerhodopsin
ChAT: choline acetyltransferase
ChR2: channelrhodopsin-2
CPA: conditioned place aversion
CPP: conditioned place preference
CTRL: control
CTXA: context “A”
CTXB: context “B”
DAB-Ni: ammonium nickel sulfate-intensified 3,3’-diaminobenzidine
DAPI: 4’,6-diaminido-2-phenylindole
DR: dorsal raphe
DTg: dorsal tegmentum
EPN: entopeduncular nucleus
eYFP: enhanced yellow fluorescent protein
FG: FluoroGold
GABA: gamma-aminobutyric acid
GFP: green fluorescent protein
FlpO: flippase enzyme
HIPP: hippocampus
IPN: interpeduncular nucleus
LC: locus coeruleus
LDTg: laterodorsal tegmentum
LH: lateral hypothalamus
LHb: lateral habenula
LPO: lateral preoptic area
Mam: mammillary body
MHb: medial habenula
MRR: median raphe region
MS: medial septum
NAcc: nucleus accumbens
NI: nucleus incertus
OFC: orbitofrontal cortex
PAG: periaqueductal grey
Pax6: paired box protein 6
PB: phosphate buffer solution
PCG: pontine central grey
PFC: prefrontal cortex
PRN: pontine reticular nucleus
PTSD: post-traumatic stress disorder
PV: parvalbumin
Reln: reelin
Reu: nucleus reuniens thalami
RmTg: rostromedial tegmentum
RTPA: real-time place aversion
RTPP: real-time place preference
Satb1: special AT-rich sequence-binding protein-1
stGtACR2: soma-targeted, *Guillardia theta* anion-conducting channelrhodopsin-2
SUM: supramammillary nucleus
SVTg. subventricular tegmental nucleus
TBS: tris-phosphate buffer solution
TH: tyrosine hydroxylase
TpH: tryptophan hydroxylase
VDB: vertical diagonal band of Broca

vGAT: vesicular GABA transporter

vGluT1/2/3: vesicular glutamate transporter type 1/2/3

VP: ventral pallidum

VTA: ventral tegmental area

ZI: zona incerta

DOI:10.14753/SE.2025.3206

1. Introduction

1.1. Emotional valence and mood regulation

Although emotion, feeling, and mood have long been studied, they do not have a single definition, and as some of the most complex higher-order brain functions, the mechanisms that contribute to their emergence are still intensely studied. Emotional episodes leave traces in the brain's affective systems, and the accumulation of these traces influences baseline mood and feelings. This is because emotional states bias perception and attention, which over time reinforce congruent mood states and influence our behavior (1). Chronic negative experiences can lead to a persistently low mood, making it easier to perceive other events negatively. Over time, this feedback loop can lead to mood-related psychiatric disorders such as depression (2,3).

1.2. Mood-related disorder: depression

The pressures of modern urban life, with its ever-increasing information overload and fast-paced, often emotionally detached social interactions, can easily disrupt our baseline mood, leading to psychiatric disorders. Currently, anxiety is the most common psychiatric disorder, with major depression being the third most common (3,4). Both disorders are becoming increasingly prevalent and represent a significant social and economic burden (5,6). Depression has a lifetime prevalence of around 15-18%, meaning nearly one in five people will experience it at some point in their lives, and it currently affects over 350 million people worldwide (3,6,7). Depressed individuals often become socially isolated and less effective at work, adding to the disorder's social and economic impact (6). Furthermore, suicidal thoughts and suicide are alarmingly common among those with depression (8). Current antidepressants are only effective for some patients, leaving many reliant on combinations of drugs and alternative treatments or without effective medications. Thus, there is still no universally effective and reliable medication for depression.

Depression is defined as a pathological shift in mood towards negativity, characterized by slowed thinking, decreased motivation, and reduced activity levels. Its development is influenced by environmental, genetic, and neurobiological factors (3,9). Depression can be categorized by severity, with minor and major forms, and by its course,

with unipolar and bipolar depression. Symptoms include a persistently low mood, anhedonia (inability to feel pleasure), more aggressive behavior, sleep disturbances, reduced concentration, fatigue, and appetite changes (3,10). Depression is significant not only because of its symptoms but also because it often coexists with other psychiatric disorders, such as anxiety in 60% of cases, and it frequently leads to physical health issues (3,11). This widespread condition imposes a growing burden on society. Understanding the biological mechanisms behind the formation of negative and positive experiences and the related mood disorders is crucial for developing more advanced therapies in the future.

1.3. General neuroanatomical background of the regulation of emotional valence

All living beings have an innate drive to seek out what is good for them and avoid what is harmful, forming coping strategies for survival (12). Basic needs such as eating, drinking, reproduction, and social interactions activate the reward system, creating positive experiences that encourage the pursuit of similar situations (13,14). In contrast, harmful environmental factors that cause tissue damage, poisoning, threats, or fear activate systems that induce disgust, avoidance, and aversion (15–17). The evaluation of experiences as positive or negative not only shapes our mood but also establishes an evolutionarily conserved balance that fundamentally influences our lives (12).

Distributed neuronal networks of the central nervous system, involving both cortical and subcortical structures, regulate the evaluation, contextualization, and cognitive control of positive and negative experiences. These valence evaluation-related brain areas are extensively studied from fishes through rodents to primates, providing insights into their anatomical and functional roles (18–20). Despite differences, many of these brain structures are evolutionarily conserved and were identified in the human brain with similar functions (19,21,22).

Positive experiences involve many brain regions, including, e.g. the ventral tegmental area (VTA), the nucleus accumbens (NAcc), the orbitofrontal cortex (OFC), the lateral habenula (LHb), and the brainstem laterodorsal tegmentum (LDTg) (14,23–25). These regions are considered to be part of the brain's reward system.

Negative experiences mostly involve other neuronal cell populations depending on the type of defensive behavior that needs to be initiated. In response to negative experiences, animals may exhibit passive or active behaviors (26,27). Passive responses

include freezing, while active responses involve "fight or flight" responses (28). Structures like the LHb, the VTA, the rostromedial tegmental nucleus (RmTg), the amygdala, the prefrontal cortex (PFC), and other forebrain regions are involved in processing negative experiences (15,23,29,30). The brainstem periaqueductal gray matter (PAG) plays key roles in executing passive fear behaviors (17,26). The septo-hippocampal system forms, stores, and recalls memories of these positive and negative experiences. Malfunctions in these brain areas are observed in various mood-related psychiatric disorders, from addictions to depression and anxiety (24,31–33). Thus, understanding the functional anatomy of these brain regions is crucial for developing treatments for these psychiatric conditions.

1.4. Ventral tegmental area: The neuronal hub for reward processing

The VTA is a dopaminergic region located in the midbrain, playing a central role in reward, reward-seeking behavior, motivation, and processing reward prediction error (20,23,30,34). The VTA receives a variety of afferent inputs from cortical, forebrain, thalamic, and brainstem nuclei, with significant contributions from the LHb, the RmTg (the primary inhibitory nucleus of the VTA), as well as the brainstem LDTg and dorsal raphe (DR) nuclei (23,29,35–38). Two major dopaminergic pathways originate from the VTA: the mesocortical pathway, which innervates the PFC and hippocampus (HIPP), and the mesolimbic pathway, which primarily targets the NAcc (23,35,39) (Fig. 1A). The VTA is highly heterogeneous in terms of its neuronal types, comprising not only dopaminergic neurons but also local γ-amino-butyratergic (GABAergic) and glutamatergic interneurons, as well as GABAergic and glutamatergic projection neurons, whose projection patterns are similar to those of the dopaminergic cells (35,40).

While stimulation of VTA dopaminergic neurons generally elicits a strong reward response, including place preference and self-administration, functional studies suggest that the role of the VTA is more complex (23,24,41). Functionally, the VTA is divided into two major regions: the medial (MVTA) and lateral (LVTA) divisions, which differentially control emotional valence (14,23,34) (Fig. 1B). LVTA dopaminergic neurons typically encode positive valence, with their firing rates increasing in response to both unpredicted and predicted rewards (23,34,42). Additionally, these neurons can code reward prediction errors, that is e.g. their activity decreases when an expected

reward is missing (Fig. 1C) or their activity increases in response to a reward that is greater than anticipated. (43,44). These reward signals from LVTA dopaminergic neurons are sent to the NAcc (23,41) (Fig. 3). However, during negative experiences, LVTA dopaminergic neurons receive inhibitory signals from local GABAergic neurons and RmTg GABAergic neurons (Fig. 3), resulting in their reduced firing rates (23,45,46). Simultaneously, MVTA dopaminergic neurons encode predominantly negative valence because their activation induces aversion, and their firing increases in response to both unpredicted and predicted aversive stimuli (23,47–49). MVTA dopaminergic neurons receive their main input from LHb glutamatergic neurons, and they relay this information to the PFC and the medial part of the NAcc (23,29,47,50) (Fig. 3). It is well established that disruptions in the dopaminergic pathways originating from the VTA are implicated in the pathophysiology of psychiatric disorders, such as addiction and schizophrenia (24,51,52). Therefore, precise regulation of VTA neurons is of paramount importance, which is strongly affected by the LHb.

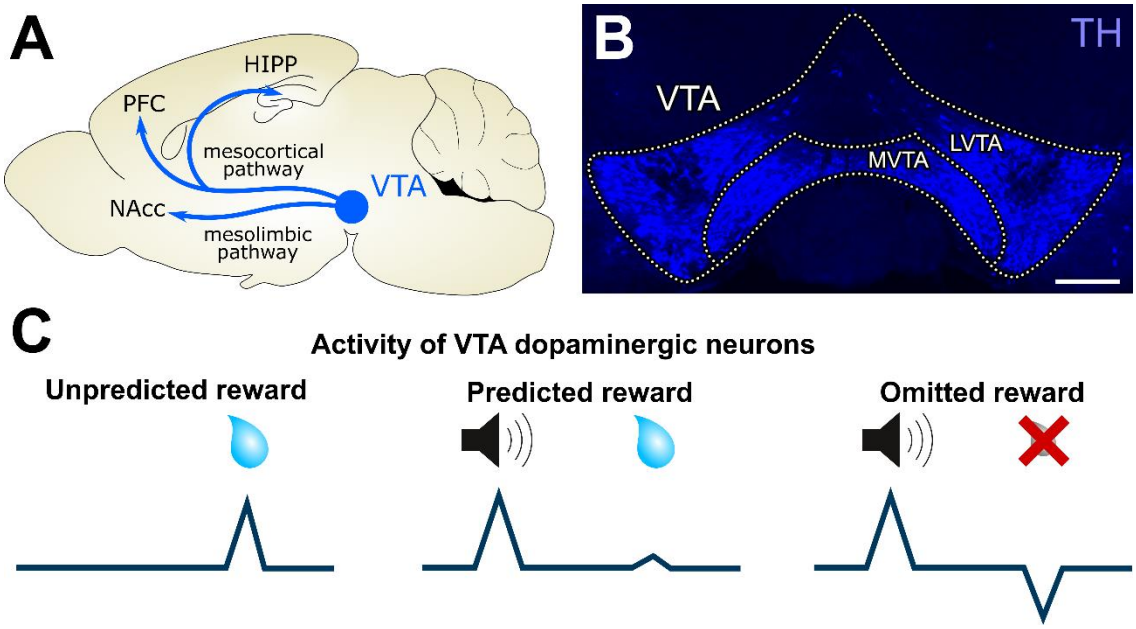

Figure 1. Functional neuroanatomy of VTA dopaminergic neurons

A: *Mesocortical and mesolimbic dopaminergic pathways arising from the VTA in mouse brain.*

B: *Two main functional divisions of the VTA (MVTA and LVTA) and the localization of the dopaminergic cells with tyrosine hydroxylase (TH) immunostaining (blue). Scale bar: 200 μm.*

C: *Schematic illustration shows how the population activity of VTA dopaminergic neurons encodes reward prediction error. (Own figure)*

1.5. Lateral habenula: The neuronal hub for processing emotional balance

The habenula is an evolutionarily ancient and conserved epithalamic structure located in the diencephalon, present from fishes to mammals, including humans (18,19). Anatomically and functionally, it is divided into two distinct parts: the medial habenula (MHb) and the lateral habenula (LHb) (18,19). The MHb receives inputs from the forebrain and transmits information to the interpeduncular nucleus (IPN) (53). Although the function of the MHb is not well understood, it is known to play a role in the development of various addictions, e.g. in nicotine withdrawal (54,55). On the other hand, the LHb is better understood and more extensively studied both in terms of its connections and its functions.

LHb neurons increase their activity in response to unexpected negative experiences or environmental cues that predict negative experiences (15,49,56). Stimulation of LHb neurons can induce place avoidance, aggression, or fear responses (e.g. freezing), depending on the environmental context (57–59). Changes in LHb neuronal signaling can also encode reward prediction error, with decreased activity observed when an expected punishment fails to occur (Fig. 2C) and increased activity in response to a punishment that is greater than anticipated. (29,44).

However, the activity of the LHb does not only encode negative emotional valence, but its neurons are also directly inhibited during rewarding or reward-predicting experiences (56,60) (Fig. 2D). Experimentally, inhibiting LHb neurons can induce place preference and reward-seeking behavior in mice (61–64). Thus, the LHb plays a central role in controlling emotional balance, which is crucial for creating appropriate survival strategies regulated by its neural inputs.

The LHb is composed almost exclusively of vesicular glutamate transporter 2 (vGluT2) positive glutamatergic neurons (46,65) (Fig. 2A). The LHb primarily receives inputs from the forebrain, including excitatory inputs from PFC, medial septum (MS), lateral preoptic area (LPO), ventral pallidum (VP), and lateral hypothalamus (LH) (19,66). It also receives mixed glutamatergic and GABAergic inputs from the entopeduncular nucleus (EPN) and the VTA, as well as afferents from the brainstem, although the neurochemical profiles of these brainstem inputs are less characterized (66–68). In return, the LHb innervates the VTA, DR, median raphe region (MRR), LDTg, nucleus incertus (NI), and the RmTg (19,69).

During a negative experience, LHb directly activates dopaminergic neurons in the MVTA, which encode aversion, and in parallel, activates GABAergic neurons in the RmTg, which inhibit dopaminergic neurons in the LVTA, which are mostly involved in reward-related behavior (23,46,59,64,70) (Fig. 2B, Fig. 3).

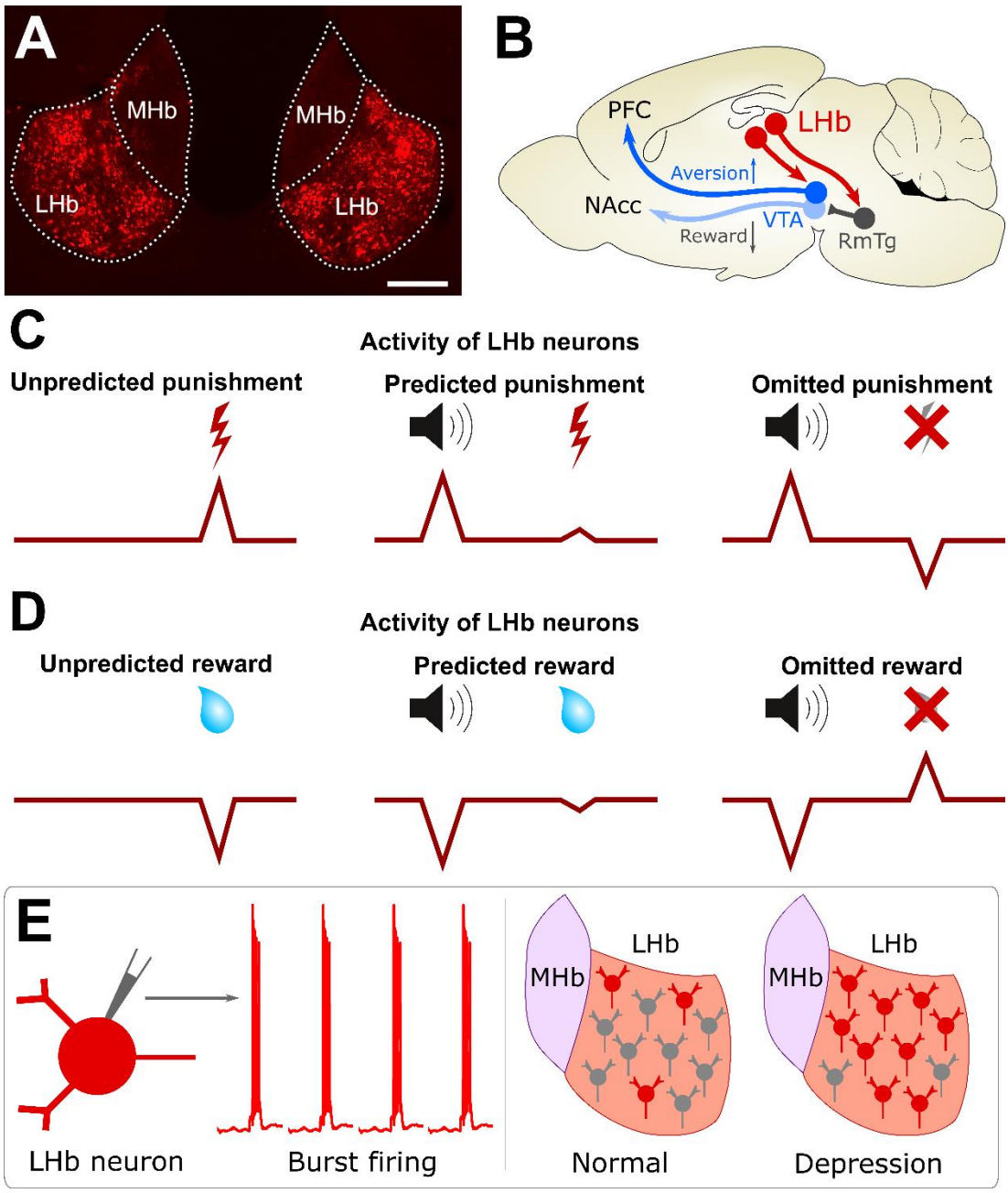

Figure 2. Functional neuroanatomy of the LHb and its role in depression

A: *Fluorescent image shows the virally labeled vGluT2 neurons in the LHb. Scale bar: 100 μm.*

B: *Illustration of the pathways originating from the LHb that regulate aversive behavior.*

C-D: *Schematic illustrations show how the population activity of LHb neurons encodes prediction errors.*
E: *Illustration of a cell exhibiting burst firing and the comparison of the number of burst-firing cells in the LHb of a normal, healthy, and a depressed mouse (based on Yang et al. 2018). (Own figure)*

It is also known that MS glutamatergic neurons can excite LHb neurons in response to negative sensory stimuli, while MS GABAergic neurons can inhibit LHb neurons in response to positive sensory stimuli (such as sweet water) (62). The LPO, VP, LH, and EPN neurons are all capable of transmitting both direct negative experiences and predictions of negative experiences to the LHb inducing avoidance in mice (61,71–73) (Fig. 3). Given the precise regulation of the LHb, it is not surprising that dysregulation of this nucleus is implicated in the development of various psychiatric disorders, from stress to depression (19,32,74–76).

1.6. The role of lateral habenula in depression

Chronic stress or excessive negative experiences can alter the characteristics of LHb neurons, potentially causing the animal to perceive even rewarding stimuli as harmful (74) and can contribute to the onset of depression (32,75,77). Chronic, elevated firing of certain (yet unknown) glutamatergic afferents to the LHb strengthens synaptic connections, leading to changes in the function of LHb neurons at the cellular level (32,78). Consequently, depression is associated with an increase in the number of LHb neurons that respond to inputs with burst firing (19,32,79). While a few neurons exhibiting burst firing are present in the LHb of healthy mice, the number is significantly higher in those suffering from depression (19,32,79) (Fig. 2E).

The LHb receives serotonergic innervation from the dorsal raphe (DR), which presynaptically inhibits glutamatergic terminals (80) that normally activate LHb neurons. This could potentially explain the effectiveness of selective serotonin reuptake inhibitors in treating depression. Moreover, the glutamatergic N-methyl-D-aspartate-receptor antagonist ketamine has been shown to significantly reduce the number of burst-firing neurons in the LHb, effectively alleviating depressive symptoms (32,79). Therefore, ketamine is the first antidepressant with a known mechanism of action. Additionally, in humans, experimental deep brain stimulation of the LHb has been found to alleviate

depressive symptoms (81,82). Moreover, the inhibitory inputs that counteract excessive excitation of the LHb could potentially be harnessed for the treatment of depression.

However, our data suggest that additional LHb inputs remain unidentified, with several ***pontine brainstem nuclei*** potentially playing a crucial role in regulating LHb circuits and associated behaviors.

1.7. Pontine brainstem role in regulating emotions

Several pontine brainstem nuclei, including the MRR, DR, LDTg, and locus coeruleus (LC), play crucial roles in regulating emotional states, mood, and the processing of positive and negative experiences (83). Previously, it was thought that the brainstem served only as a slow, modulatory center (83), but recent studies -including those carried out in our laboratory- suggested that brainstem neurons can influence cognitive functions through fast synaptic transmission (84–86). Raphe nuclei are key sources of serotonin, a neurotransmitter deeply involved in mood regulation and the stress response, which is why dysregulation in these areas is often linked to depression and anxiety (87–90). The DR serotonergic fibers innervate almost the whole brain, from the cortex to various subcortical structures, modulating functions from sleep-wake cycles to fear and reward regulation (91–93) (Fig. 3). Nevertheless, DR vGluT3 positive glutamatergic cells directly innervate the LVTA dopaminergic neurons, contributing to the experience of positive events (37). Although the MRR was previously thought to be a serotonergic nucleus, 62% of its neurons are GABAergic local interneurons (94). Only 2% of the identified projection neurons of the MRR are purely serotonergic; the rest are either vGluT3-positive glutamatergic (3.5%) or mixed serotonergic/vGluT3-positive neurons (7%) (94). MRR projection neurons extensively innervate regions involved in memory formation, such as the PFC and the septo-hippocampal system (84,85,95) (Fig. 3). Additionally, 26% of the neuronal types of the MRR remained unidentified, with their functions still unknown (94).

DOI:10.14753/SE.2025.3206

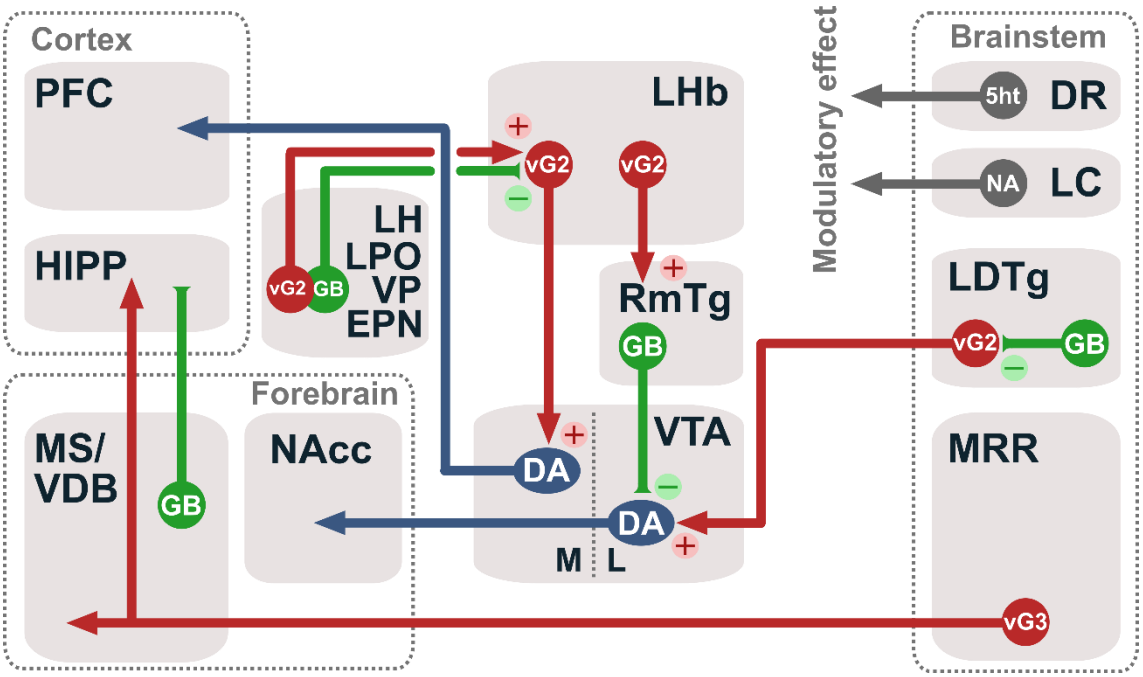

Figure 3. Illustration of the anatomical connectivity of brain regions involved in regulating emotional balance. *Abbreviations: 5ht: serotonin, DA: dopaminergic neurons, GB: GABAergic neurons, NA: noradrenaline, vG2/vG3: vGluT2/vGluT3. (Own figure)*

The LC (like the DR) sends widespread but less specific noradrenergic projections across the brain, influencing arousal, vigilance, and stress responses, with its overactivity contributing to anxiety disorders (96,97) (Fig. 3). The cholinergic and glutamatergic neurons of the LDTg innervates the reward system, including LVTA dopaminergic neurons and the nucleus NAcc, while its heterogeneous GABAergic neurons, through local collaterals and inhibition of the LVTA, primarily encode negative experiences (23,25,36,98,99) (Fig. 3). Therefore, the LDTg is involved in reward processing and motivational states, regulating the emotional balance.

Dysfunction in these brainstem regions can disrupt the delicate balance of neurotransmitter systems, leading to the development of psychiatric disorders such as depression and anxiety (83,100–102). However, our knowledge of the brainstem remains incomplete. While it is evident that the brainstem can influence various emotion and mood-related functions, its connections with the LHb are still poorly understood.

2. Objectives

This thesis aimed to investigate the brainstem's role in modulating LHb during aversive and rewarding events.

2.1. Excitatory Innervation to the LHb from the Brainstem

The LHb plays a central role in evaluating and predicting adverse events, with dysfunction being associated with depression. However, the neuronal mechanisms underlying LHb activation and aversive information relay remain poorly understood. The median raphe region (MRR) in the brainstem is well-positioned to provide rapid and coordinated excitation of the LHb during adverse events.

2.1.1. What is the largest projecting neuronal population in the MRR?
2.1.2. Where do these MRR neurons project to?
2.1.3. Which brain areas provide input to these MRR neurons?
2.1.4. How does the stimulation of these MRR neurons affect the mouse behavior?
2.1.5. When a negative memory trace is forming, is the function of these MRR neurons necessary for the formation of a proper fear memory?

2.2. Inhibitory Innervation to the LHb from the Brainstem

Inhibition of the LHb can signal positive valence and reward and is critical for behavioral flexibility and decision-making. Despite decades of research, inhibitory inputs to the LHb remain poorly characterized, and no inhibitory connections from the brainstem have been identified to date. This objective aims to explore the following:

2.2.1. Which neurons provide the primary inhibitory input to the LHb?
2.2.2. Are these neurons located in the brainstem?
2.2.3. How does the stimulation or inhibition of these inhibitory neurons affect mouse behavior?
2.2.4. Which neuronal inputs control the activity of these inhibitory neurons?
2.2.5. Are there molecular markers that can uniquely identify these inhibitory neurons?
2.2.6. Are similar neuronal populations present in humans?

3. Methods

3.1. Ethical consideration

All experiments were performed in accordance with the Institutional Ethical Codex and the Hungarian regulations on animal research (Act XXVIII of 1998, Government Decree 40/2013), in line with the EU Directive 2010/63/EU. The Animal-welfare Body of the Institute of Experimental Medicine and the Government Office of Pest County authorized the experiments at project numbers PEI/001/33-4/2013, PE/EA/2553-6/2016, PE/EA/254-7/2019, and PE/EA/00063-5/2022.

3.2. Mice and rats

We used vGAT-iRES-Cre (Stock No.: 016962), vGluT1-iRES-Cre (Stock No.: 023527), vGluT2-iRES-Cre (Stock No.: 028863), vGAT-iRES-flpo (Stock No.: 029591), Gt(ROSA)26Sor-CAG/LSL-ZsGreen1 (Stock No.: 007906) mice (all from The Jackson Laboratory). We also crossbred mice to create vGAT-iRES-flpo/vGluT2-iRES-Cre and vGAT-iRES-Cre/Gt(ROSA)26Sor-CAG/LSL-ZsGreen1 mice. We used adult (at least 6 weeks old) mice from both sexes in our experiments. Mice had access to food and water ad libitum and were housed in a vivarium (3-5 mice/cage) until used in experiments. Mice used for optogenetic behavioral experiments were maintained on a normal 12h light-dark cycle, with experiments performed during the light phase of the cycle.

The same adult male Wistar rats were previously studied by Szabadits et al. in 2007 (103). Here, we investigated the stored brainstem blocks of one of those Wistar rats. All Experiments were performed in accordance with the Institutional Ethical Codex and the Hungarian Act of Animal Care and Experimentation guidelines, which are in concert with the European Communities Council Directive of November 24, 1986 (86/609/EEC).

3.3. Macaque monkey

The same adult female rhesus macaque monkeys (*Macaca mulatta*) were previously studied by Rovo et al. in 2012 (104). Here, we investigated the stored brainstem blocks of two of those monkeys. All experimental procedures were performed according to the ethical guidelines of the Institute of Experimental Medicine and Institute

of Physiology of the Hungarian Academy of Sciences and were approved by the Ethical Committee (Approval 22.1/77/001/2010).

3.4. Human samples

Human brainstem and hippocampus samples were obtained from two subjects who died due to causes not directly involving any brain disease or damage and without having a medical history of neurological or psychiatric disorder. All procedures were carried out in compliance with the Declaration of Helsinki and were approved by the Regional Committee of Science and Research Ethics of the Scientific Council of Health (ETT TUKEB 31443/2011/EKU, renewed: BM/15092-1/2023). The subjects went through an autopsy in the Department of Pathology of St. Borbála Hospital, Tatabánya, Hungary. Informed consent by relatives was obtained for the use of brain tissue and access to medical records for research purposes. Samples from the following subjects were used in the present study: SKO28 (pontine samples): 93 years old, female, post-mortal time (PMI): 3h 44 min, right side of the brainstem; SKO30 (pontine samples): 63 years old, female, PMI: 3h 45 min, whole pons and left side hippocampal slice. Brains were removed after death, and the internal carotid and vertebrate arteries were cannulated. First, physiological saline containing 0.33% heparin was perfused through this system (1.5 l in 30 min), after which perfusion continued with Zamboni fixative solution containing 4% paraformaldehyde and 0.2% picric acid in 0.1 M phosphate buffer (PB, pH = 7.4, 2 h, 4 l). PMI was determined between the time of death and the start of perfusion by Zamboni fixative.

3.5. Stereotaxic surgeries for viral gene transfer, retrograde tracing, and optic fiber implantation in mice

Mice were anesthetized with 2.5% isoflurane vapor followed by an intraperitoneal injection of an anesthetic mixture (containing 8.3 mg/ml ketamine and 1.7 mg/ml xylazine-hydrochloride in 0.9% saline, 10 ml/kg body weight) or maintained the anesthesia with 1-1.5% isoflurane; and were then mounted in a small animal stereotaxic frame and the skull surface was exposed. A Nanoject II precision microinjector pump was used for the microinjections. Before virus injection, mice received 0.03 ml 10% buprenorphine solution subcutaneously to minimalize postoperative discomfort. For viral

labeling experiments, we injected 20-100 nl of one of the used virus preparations (Table 1) into the target brain areas. The titers of the used viruses were between 4-70×10^{12} colony forming units/ml. The coordinates for the injections were defined by a stereotaxic atlas; the null coronal plane of the anteroposterior (AP) axis was defined by the position of Bregma; the null sagittal plane of the mediolateral (ML) axis was defined by the superior sagittal sinus; the null horizontal plane of the dorso-ventral (DV) axis was defined by the positions of Bregma and Lambda points. The injection coordinates were the following (always given in mm at the AP, ML and DV axes, respectively): MRR: -4.5, 0.0, -4.5; MRR for stereology (4 injections altogether): -4.3, 0.0, -4.3 and -4.8 and -4.7, 0.0, -4.1 and -4.6; LHb: -1.6, +/- 0.4, -2.8; HIPP: (2-2 injections bilaterally) -2.0, +/- 1,5, -2 and -2.7, +/- 2.5, -2.7; SVTg: -5.2, +/-0.4, -3.6; VTA: -3.3, +/-0.4, -4.2; OFC: +2.6, +/-0.6, -2.5. After the surgeries, mice received 0.3-0.5 ml saline and 0.1 mg/kg meloxicam intraperitoneally and were placed into separate cages until further experiments or perfusions.

Table 1. Viral constructs

Virus type	**Source**	**Identifier**
AAVretro-hSyn-DIO-eGFP	Addgene	50457-AAVrg
AAVretro-EF1α-DIO-mCherry	UNC Vector Core	50459-AAVrg
AAVretro-EF1α-DIO-ChR2-mCherry	Addgene	20297-AAVrg
AAVretro-hSyn-SIO-stGtACR2-FusionRed	Addgene	105677-AAVrg
AAVretro-hSyn-FLEX-jGCaMP8m	Addgene	162378-AAVrg
AAVretro-EF1α-DIO-FlpO	Addgene	87306-AAVrg
AAVretro11-EF1α-DIO-GCaMP6m	Braincase	Custom made
AAV2/5-EF1α-DIO-eYFP	UNC Vector Core	27056-AAV5
AAV2/5-EF1α-DIO-mCherry	UNC Vector Core	Plasmid #50462
AAV2/1-EF1α-fDIO-mCherry	Addgene	114471-AAV1
AAV2/5-EF1α-DIO-hChR2(H134R)-eYFP	UNC Vector Core	20298-AAV5
AAV2/9-EF1α-DO-ChR2-mCherry	Salk GT3 Vector Core	Plasmid #37082
AAV2/8-hSyn-FLEX-TVA-p2A-eGFP-p2A-oG	Salk GT3 Vector Core	Plasmid #85225
RabiesΔG-EnvA-mCherry	Salk GT3 Vector Core	Plasmid #32636
AAV2/9-hSyn-FLEX-TVA-oG-nlsGFP-WPRE3	Charité Universitätsmedizin Berlin Viral Core Facility	BA-96 AAV2/9
RabiesΔG-EnvA-mCherry		BRABV-001

For behavioral optogenetic experiments, virus injections were followed by optic fiber surgeries. These were similar to virus injections and were carried out 5-6 weeks after virus injections. Optic fibers for behavioral experiments had 105 μm core diameter for all MRR behavioral and SVTg RTPP experiments, or 200 μm core diameter for all other SVTg behavioral experiments (0.22 NA, Thorlabs), which were implanted into the brain with the tip at the following coordinates (always given in mm at the AP, ML, and DV axes, respectively): MRR: -4.5, 0.0, -4.4; SVTg: -5.3, +0.4, -3.1 or 20 degree coronally angled -5.3, +1.6, -2.7; LHb: -1.8, +0.4, -2.1 or 20 degree coronally angled -1.8, +1.25, -1.8. For secure fixture of the implantable optic fiber and a head-plate for head-fixation, the surface of the skull was disinfected and dried with 70% ethanol, then a three-component Super-Bond was added into the skull and finally dental cement was added between the Super-Bond and the base of the ceramic ferrule of the fiber implant. Injection sites and the positions of the optic fibers are reconstructed after the experiments. After the surgeries, mice received 0.3-0.5 ml saline and 0.1 mg/kg meloxicam intraperitoneally and were placed into separate cages until experiments.

3.6. Mono-transsynaptic rabies tracing

A detailed description of the monosynaptic rabies tracing technique used has already been published (105). Briefly, vGluT2-Cre or vGAT-Cre mice were prepared for stereotaxic surgeries as described above, and 30-80n nl of the helper virus was injected into the MRR or SVTg, respectively, at the coordinates given above. These Cre-dependent viruses express the avian tumor virus receptor A (TVA), which enables neurons to be infected by rabies viruses. Additionally, they carry an upgraded version of the rabies glycoprotein (oG), enhancing the trans-synaptic labeling efficiency of the rabies viruses (106). After 2-5 weeks of survival, mice were injected with the genetically modified rabies at the same coordinates in case of the MRR, or into the LHb. After 7-10 days of survival, mice were prepared for perfusions.

3.7. Perfusion and sectioning

Mice were anesthetized with 2% isoflurane vapor followed by an intraperitoneal injection of an anesthetic mixture (containing 8.3 mg/ml ketamine, 1.7 mg/ml xylazine-hydrochloride, 0.8 mg/ml promethazinium-chloride) to achieve deep anesthesia. Mice

were then perfused transcardially with 0.1M phosphate-buffered saline (PBS, pH 7.4) solution for 2 min, followed by 4% freshly depolymerized paraformaldehyde (PFA) solution for 45 min, followed by PBS for 10 min, then the brains were removed from the skull. After perfusions, brains were cut into 50-60 μm-thick coronal sections using a vibrating microtome.

3.8. Antibodies

The list of the primary and secondary antibodies used can be found in Table 2-3. The specificities of the primary antibodies were extensively tested, using either knock-out mice or other reliable methods. Secondary antibodies were extensively tested for possible cross-reactivity with the other antibodies used, and possible tissue labeling without primary antibodies was also tested to exclude auto-fluorescence or specific background labeling. No specific-like staining was observed under these control conditions.

3.9. Fluorescent immunohistochemistry, epifluorescent and laser-scanning confocal microscopy for counting cells and synaptic contacts

Perfusion-fixed sections were washed in 0.1 M PB (pH 7.4) and incubated in 30% sucrose overnight for cryoprotection. Sections were then freeze-thawed over liquid nitrogen three times for antigen retrieval. Sections were subsequently washed in PB and Tris-buffered saline (TBS, pH 7.4) and blocked in 1% human serum albumin in TBS, and then incubated in a mixture of primary antibodies for 48-72 h. This was followed by extensive washes in TBS, and incubation in the mixture of appropriate secondary antibodies overnight. In some cases, we used 4’,6-diaminido-2-phenylindole (DAPI) staining to visualize cell nuclei. Then, sections were washed in TBS and PB, put on slides, and covered with Aquamount. For the behavioral optogenetic and for viral anterograde and retrograde tracing experiments, each injection site was reconstructed from 50-60 μm sections using an epifluorescent Zeiss Axioplan2 microscope. Every part of the injected tissue containing even low levels of tracer was considered as part of the injection site. For anatomical analyses, sections were evaluated using a Nikon A1R confocal laser-scanning microscope system built on a Ti-E inverted microscope with a 4× or 10× or 20× air objective or with a 1.4 NA CFI Plan Apo VC 60× oil objective both operated by NIS-

Elements AR 4.3 software. Regions of interest were reconstructed in z-stacks; the distance between the focal planes was 0.3-0.5 µm for examined synaptic contacts and 2-3 µm for examined neuronal somata. The cell and synaptic counting were performed using the NIS-Elements AR 4.3 or Adobe Photoshop CS6 Extended software. All anatomical measurements and investigations were done from at least 2 mice.

Table 2. Primary antibodies

Antigen or reagent	Host	Dilution	Source	Catalog#
Cav3.1	Mouse	1:100	UC Davis/NIH NeuroMab Facility	75-206
ChAT	Rabbit	1:1000	Synaptic Systems	297013
eGFP	Chicken	1:2000	ThermoFisher Scientific	A10262
FluoroGold (FG)	Guinea pig	1:5000	Protos Biotech Corp	NM-101
Gephyrin	Rabbit	1:2000	Synaptic Systems	147 008
Homer-1	Rabbit	1:2000	Synaptic Systems	160003
mCherry	Rabbit	1:2000	BioVision	5993-100
Parvalbumin	Mouse	1:2000	Swant	235
Pax6	Rabbit	1:500	ThermoFisher Scientific	42-6600
Reelin	Goat	1:200	ThermoFisher Scientific	PA5-47537
RFP	Rat	1:2000	Chromotek	5F8
Satb1	Mouse	1:500-1:1000	SantaCruz Biotechnology	sc-376096
TH	Mouse	1:2000	ImmunoStar	22941
TpH	Mouse	1:3000	Sigma-Aldrich	T0678
vGAT	Guinea pig	1:2000	Synaptic Systems	131 004
vGluT2	Guinea pig	1:2000	Synaptic Systems	135 404
vGluT2	Rabbit	1:2000	Synaptic Systems	135 402
vGluT3	Rabbit	1:400-1:1000	Synaptic Systems	135 203
DAPI		1:10000	Sigma-Aldrich	32670
FluoroGold (FG)		2%	FluoroChrome Inc.	-

Table 3. Secondary antibodies

Raised in	Raised against	Conjugated with	Dilution	Source	Catalog#
Donkey	Rabbit	Alexa 647	1:500	Jackson Immunoresearch	711-605-152
Donkey	Mouse	Alexa 647	1:500	Jackson Immunoresearch	715-605-151
Donkey	Guinea pig	Alexa 647	1:500	Jackson Immunoresearch	706-605-148
Donkey	Goat	Cy5	1:500	Jackson Immunoresearch	705-175-147
Goat	Chicken	Alexa 488	1:1000	ThermoFisher Scientific	A11039
Donkey	Chicken	Alexa 488	1:1000	Jackson Immunoresearch	703-545-155
Goat	Guinea pig	Alexa 488	1:500	ThermoFisher Scientific	A11073
Donkey	Goat	Alexa 594	1:500	ThermoFisher Scientific	A11058
Donkey	Rabbit	Alexa 594	1:500	ThermoFisher Scientific	A21207
Donkey	Rat	Alexa 594	1:500	ThermoFisher Scientific	A21209
Donkey	Mouse	Alexa 594	1:500	ThermoFisher Scientific	A21203
-	-	DyLight405	1:500	Jackson Immunoresearch	016-470-084
Horse	Mouse	biotinylated	1:500	Vector Laboratories	BA-2000

3.10. Stereological measurement

We labeled every second section of the excised brain sections with fluorescence. The stereological counting was performed using the optical fractionator method, which is based on the principle that one can accurately define the number of cells in the volume of interest by counting them in a predetermined fraction of the given volume (107,108). To get the total number of cells a back-calculation was performed in three steps (109): first, for the entire thickness of the section, then for the total area of the MRR on the given section, and finally for all sections of the MRR. Cell counting was conducted using the Stereo Investigator 10.0 software, and cell identification was carried out using the NIS-Elements software. Initially, using the software and the anatomical atlas, we traced the MRR. Then, a 5μm safety zone was applied at the top and bottom of the sections, and the area was divided into smaller 80 μm² regions, within each of which cells were counted in a 10 μm² area (for paramedian raphe) and a 15 μm² area (for median raphe) located in the upper left corner. The cell back-calculation was performed based on the previous steps. Finally, based on the known cells and the group's previous, more detailed measurements, the obtained ratio was used to multiply the number of vGluT2-positive cells, which

allowed us to determine the total number of vGluT2-positive cells in the MRR in the mouse brain.

3.11. Immunoperoxidase staining and imaging for rat, macaque, and human brain slices

Perfusion-fixed (4% PFA, 0.5% glutaraldehyde) macaque brainstems (kind gift from László Acsády) were embedded into 2% agarose and were cut into 80 µm-thick coronal sections using a vibrating microtome. Perfusion-fixed human brainstems were embedded into 3% agarose and were cut into 80 µm-thick coronal sections using a vibrating microtome. These sections were washed in 0.1 M PB (pH 7.4) and incubated in 30% sucrose overnight for cryoprotection. Sections were then freeze-thawed over liquid nitrogen three times for antigen retrieval. After subsequent wash in PB, sections were incubated in 100x citrate buffer (pH 6.0) at 80 Celsius degree for 30 minutes. Then sections were washed in PB (2×10 min) and treated with 1% sodium borohydride in PB for 15 min. After extensive washes in PB (5×5min) endogenous peroxidase-like activity was blocked by 1% H_2O_2 in TBS for 10 min. Then sections were transferred into 0.05 M TBS (pH 7.4) and blocked in 2% bovine serum albumin and 0.1 g/ml lysine and glycine in TBS. Then, sections were incubated without primary antibodies (CTRL staining) or in a solution of mouse anti-Satb1 or rabbit anti-ChAT primary antibodies diluted in TBS. After repeated washes in TBS, the sections were incubated in biotinylated secondary antibodies overnight followed by extensive washes in TBS (3×10 min) and in avidin–biotinylated horseradish peroxidase complex for 3 h (1:300 in TBS; Standard ABC, Vector Laboratories). The immunoperoxidase reaction was developed using ammonium nickel sulfate-intensified 3-3’-diaminobenzidine (DAB-Ni) as the chromogen. After washes in PB, sections were contrasted with 0.25% osmium-tetroxide in PB on ice for 10 min. The sections were then dehydrated in ascending alcohol series and in acetonitrile and embedded in Durcupan (ACM; Fluka). The same protocol was used for rat slices. For imaging, we used a Zeiss Axioplan2 microscope in bright field mode.

3.12. Real-time and conditioned place preference (RTPP, CPP) or aversion (RTPA, CPA) tests

After optic fiber implantations, mice were transferred to an animal room in the behavioral unit of the institute to rest, then they received 5 days of handling. On the 6th day (habituation day), mice were placed into a box (40 cm x 20 cm x 20 cm, divided into two chambers with striped walls and floor on one side and dotted walls and floor on the other side (CPA box) and were allowed to freely move for 10 minutes. After each experiment, the box was washed with “argan oil-scented” soap. On the 7th day (real-time place preference (RTPP) / real-time place aversion (RTPA)), mice were placed back into the CPA box for 10-15 minutes. They received light illuminations via the optic fibers either for stimulation (in the case of the MRR 5ms pulses at 25 Hz with 10-15mW intensity, 473 nm; in the case of the SVTg 10 ms pulses at 20 Hz, 8-10 mW intensity, 473 nm) or inhibition (continuous, 8 mW intensity, 473 nm) of the target areas when they entered one side of the box. On the 8th day (conditioned place aversion/conditioned place preference), mice were tested without light illuminations for 5-10 min in the same box. The experiments were performed in a counter-balanced way; some mice received light illuminations on the striped side, while others received them on the dotted side, to exclude the possibility of innate aversion/preference for any context.

To precisely examine whether mice distinguished the stimulated and non-stimulated sides in the RTPP/RTPA and CPP/CPA paradigms, the box was divided into three virtual areas: an optic fiber illumination area, a non-illuminated area, and a so-called decision zone. The decision zone was a rectangle with an area of 14 cm x 8 cm (14% of the total box area of 800 cm^2) placed in the middle of the box. We excluded the time spent in the decision zone to exclude any possible uncertainty of the detection of the position of the mice in the middle of the box. To define the percentage of time spent by the mice in the different contexts, we divided the time spent in the stimulation area by the sum of the time spent in the stimulation area plus the non-stimulated area.

3.13. Aversive operant conditioning test

On the 9th day (after RTPA and CPA tests in the case of the MRR experiments), mice were put on a restrictive diet: ad libitum food was removed, and mice were provided with 1.5-2.5 g of food pellets daily. The restricted diet allowed subjects to maintain 80-

90% of their initial weight while promoting motivation to explore the environment, thus increasing responsivity during the task. They were also habituated to the reward pellets used in the operant conditioning paradigm for 3 days. The diet was held for the whole duration of the operant conditioning tests to support the motivational drive to poke for pellet rewards. On the 12th day, mice were put in an automated operant conditioning chamber system, and they were conditioned to nose-poke for pellet rewards (45mg) for 30 minutes/day for 10 days. The chamber was put in a dark box, but it was lit by a house light. Every correct nose-poke was followed by a 15-second-long interval when the house light turned off and mice did not receive pellet rewards even if they performed nose-pokes. This interval was inserted into the experiment to help the mice learn the conditioning rule, and to allow them time to consume the pellets. After this interval, mice could perform a correct nose-poke again to receive pellets. The number of total nose-pokes was defined as the sum of the correct nose-pokes and the interval nose-pokes. The operant conditioning chambers were washed after every individual mouse with distilled water. From the 20th day, mice were connected to a dummy fiber patch for habituation. On the 22nd day (poke stimulation), mice received 5 seconds of blue laser stimulation (5 ms pulses at 25 Hz with 10-15mW intensity, 473 nm) after every correct nose-poke. After the 30-minute stimulation period, mice were placed back into their home cages and received food ad libitum again for 3 days to regain their original weight.

We compared the number of total nose pokes performed by the individual mice in a pairwise manner between the 21st (baseline performance) and 22nd (stimulation) days of the experiment. Then, we normalized the number of the total nose-pokes performed by a mouse on the 22nd day to the number of the total nose-pokes performed by the same mouse on the 21st day, respectively (Poke ratio, stimulation/base). These ratios were compared between the groups of channelrhodopsin-2 (ChR2) mice and control (CTRL) mice.

3.14. Operant self-stimulation test

After optic fiber implantations, mice were transferred to an animal room in the behavioral unit of the institute to recover and acclimatize, then they received 5 days of handling. Three days before testing, mice were started to be kept on a diet to keep their body weight between 80%-90% of the original to promote motivation to explore the

environment, thus increasing responsivity during the task (see above). The operant discrimination task was performed in daily sessions using automated operant chambers equipped with two nose-poke response holes with infrared sensors and LED cue lights. All chambers were surrounded by ventilated, sound-attenuating cubicles and controlled by MED-PC V software. At the beginning of the session, ferrules were connected to the optical fibers, which were connected to the lasers, and mice were placed in the operant chambers. At startup, cue lights in the nose poke response holes were on, house lighting was off. Nose poke response on the active ILLUM hole resulted in a 2-second-long laser stimulation (473nm, delivered at 10-12 mW, 10 ms pulse width at 20 Hz on the first 3 days and 40 Hz on the other days) elicited via a TTL adapter connecting the chamber to the laser apparatus. Stimulus presentation was followed by a 5-second-long inter-trial interval (ITI) with the house light on and cue light off, during which responses resulted in no effect. Response on the inactive nose poke response hole (NON) had no effect at any point of the session. The designation of the active nose-poke response hole side was randomly determined between subjects and was constant within one subject throughout the whole experiment. Every session lasted 30 minutes, after which subjects were returned to their home cages and provided with their daily food pellets. Operant chambers were cleaned with water between subjects and dried with a paper towel. On the last day of the session, mice did not receive laser stimulations, so we tested their memory of the previous day. Registered variables were the number of responses on active and inactive nose-poke response holes, responses during stimulus presentation and ITI, total number of responses, and preference towards responding on the active response hole in % of all responses (responses on active hole / (responses on active hole + responses on inactive hole) * 100). We analyzed and drew conclusions from the number of all nose-pokes number either from the illuminated side (ILLUM) or the non-illuminated side (NON) and the preference on each day.

3.15. Cued fear conditioning test

After optic fiber implantations, mice were transferred to the animal room of the behavioral unit, where they received 5 days of handling. On the 6th day, mice were placed into the first environmental context (context “A”: CTXA) in a plexiglass shocking chamber (25cm×25cm×31cm) that was enriched with a specific combination of olfactory

(macadamia nut scent), visual (black dotted wall with white background), spatial (bent chamber walls), auditory (white noise) and tactile (metal bars on the floor) cues. Mice were allowed to freely move in the first environment for 3 minutes to record baseline freezing levels. After this, mice received 3 shocks (2 seconds, 2 mA intensity, 60 seconds inter-shock interval) that were paired with an auditory cue (30 seconds long sound at 7500 Hz). The foot shocks and the auditory cues were co-terminated each time. Foot shocks were paired with 6 seconds-long yellow laser light illumination (continuous, 10-15 mW, 593 nm), which was precisely aligned with the shocks, starting 2 seconds before the shock onset and finishing 2 seconds after the shock offset. After receiving the last shock, mice were kept in the context for another 30-60 seconds. After 3 successfully delivered shocks, mice were placed back into their home cages for 24 h. On the 7th day, mice were placed back into the CTXA for 3 minutes to record freezing behavior related to contextual fear memories. 24 hours later, on the 8th day, mice were placed into a second environmental context (context “B”: CTXB) with distinct olfactory (citrus scent), visual (black and white striped wall), spatial (square-shaped chamber), auditory (no noise) and tactile (plastic floor) cues. For 3 minutes, generalized fear levels were recorded in CTXB. After this, mice were presented with the auditory cue for 1 minute to record freezing behavior related to the cued fear memories. After the termination of the auditory cue, mice were kept in the CTXB for 1 minute to read out post-cue freezing levels. The behavior of mice was recorded with a Basler acA1300-60gc camcorder and freezing behavior was analyzed manually using the Solomon Coder software. The experimenter evaluating freezing levels was blind to the conditions and treatment of the mice. Mice displaying higher than 5% baseline freezing levels (before foot shocks) in CTXA were excluded from further analysis.

3.16. Contextual fear conditioning test

In the case of the SVTg inhibition experiment, after place aversion tests mice rested for 3 days. On the 12th day (Shock + Light), mice were placed into a plexiglass foot-shock chamber (25cm×25cm×35cm) that was enriched with a specific combination of olfactory (citric soap scent), visual (white walls), spatial (rectangular chamber walls) and tactile (metal bars on the floor) cues (context “A”: CTXA). Mice were allowed to freely move in the environment for 3 minutes and we recorded their baseline freezing

levels. After this, mice received 4 foot shocks (2 seconds long, 2 mA, 60 seconds inter-shock interval). Mice received light illuminations precisely aligned to the shocks, starting 2 seconds before the shock onset, and finishing 2 seconds after shock termination (continuous, 8 mW, 473 nm). After receiving the last illumination, mice were kept in the context for another 1 minute. 24 hours later, in the morning, mice were placed back into CTXA for 5 min without light illuminations to measure their freezing levels (contextual fear readout). In the afternoon, 4-5 hours after context readout, mice were placed into a different chamber, CTXB (rat foot shock chamber, grey curved walls, darker ambient light, washed with baby soap scent) for 5 min without light illuminations to read out their freezing levels (generalized fear readout).

The behavior of the mice was recorded with a Basler acA1300-60gc camcorder, and the freezing behavior of mice was recorded with a custom-made freezing detection head-mounted sensor. Motionless periods needed to be at least 2 seconds long to be considered freezing behavior.

3.17. Analysis and statistics for behavioral experiments

The experimental data was collected and analyzed using the Noldus EthoVision 15.0 and Tibco Statistica 13.4 software in the case of all behavioral experiments. All behavioral experiments were performed with at least 2 different cohorts of mice, except for the self-stimulation experiment (1 cohort). In the case of data groups that did not show a Gaussian distribution, we used median and 25% to 75% interquartile range to present data. Homogeneity of variance was tested using F-test and if it was significant then populations were compared using nonparametric tests. To test for statistical differences, we used the nonparametric Mann–Whitney U-test or parametric Student’s t-test in independent data populations, we used the Wilcoxon’s signed-rank test in nonparametric dependent data populations. Statistical differences have always been tested using two-sided tests. For indicating significance levels on figures, we used the following standard rules, n.s. (non-significant): $p > 0.05$, *: $p < 0.05$, **: $p < 0.01$, ***: $p < 0.001$, ****: $p < 0.0001$.

4. Results

4.1. Excitatory innervation to the LHb from the Brainstem

4.1.1. vGluT2 neurons are the largest population of projection cells in the MRR

The transmitter phenotypes of almost 25% of MRR neurons were unknown (94). By injecting a large amount of AAV2/5-EF1α-DIO-eYFP Cre-dependent virus into the MRR of vGluT2-Cre mice and then performing quantitative stereological measurements, we found that at least 20% (from 3 mice) of the neurons in the MRR were vGluT2-positive glutamatergic cells (Fig. 4A, Table 4). Based on our fluorescent labeling, we observed that MRR vGluT2 neurons are completely distinct from the previously known serotonergic (5HT) and vGluT3 positive glutamatergic cells in the MRR (Fig. 4B). We also found that MRR vGluT2 neurons send dense axonal arborization to the forebrain, especially to the LHb. Our anatomical analysis of virally labeled MRR vGluT2-positive axon terminals in the LHb revealed that at least 93% (339/367 terminals from 2 mice) of eYFP-labeled MRR terminals were clearly immunopositive for vGluT2, but were not positive for vGAT (6/200 terminals from 2 mice) and for vGluT3 (2/200 terminals from 2 mice) (Fig. 4C-D). These data show that vGluT2 neurons are distinct from other cell types in MRR and represent the largest population of projection neurons in MRR.

4.1.2. MRR vGluT2 neurons innervate aversive and memory formation-related nuclei

Next, we investigated the axonal projection of MRR vGluT2 neurons in the whole brain, especially those that project to the LHb. Therefore, we performed intersectional viral tract tracing by injecting a retrogradely transmitted Cre-dependent flippase (FlpO) encoding virus into the LHb and then injecting a Cre- and Flp-dependent (AAV/DJ-hSyn-CreON/FlpON-ChR2-eYFP) virus into the MRR of vGluT2-Cre mice (Fig. 4E-F). We found that LHb-projecting MRR vGluT2 neurons do not only innervate the LHb, but also send axonal collaterals to other valence-processing-related subcortical brain areas [to the LH, the LPO, the DR, the pontine central grey (PCG), the VTA and the IPN] and the same MRR cells also innervate the memory-processing-related basal forebrain [medial septum/vertical diagonal band of Broca (MS/VDB)] (Fig. 4G).

DOI:10.14753/SE.2025.3206

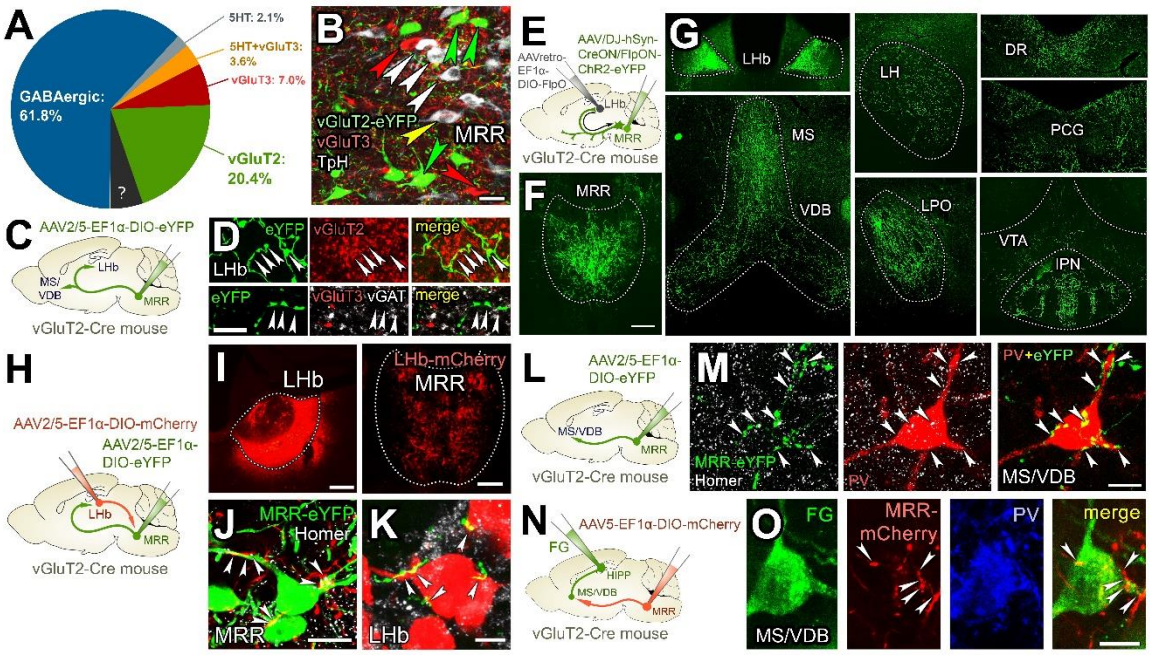

Figure 4. Anatomical details of MRR vGluT2 neurons

A: *The pie chart shows that at least 20% of the MRR neurons are vGluT2-positive. For stereological statistical details, see Table 4.*

B: *Virally labeled (with AAV2/5-EF1α-DIO-eYFP in vGluT2-Cre mouse) vGluT2-positive (green arrows), immunolabeled vGluT3-positive (red arrows), TpH-positive and TpH/vGluT3 double-positive cells in MRR. Scale bar: 20 µm.*

C: *AAV2/5-EF1α-DIO-eYFP was injected into the MRR of vGluT2-Cre mice (n=2).*

D: *Representative confocal-laser scanning images from LHb show that eYFP-labeled MRR fibers (green) are indeed immunopositive for vGluT2 (red, upper panel), but not positive for vGAT (white) or vGluT3 (red, lower panel). Scale bar: 10 µm.*

E: *Cre-dependent Flp-expressing colorless retrograde AAV (AAVretro-EF1α-DIO-FlpO) was injected into the LHb, and Flp- and Cre-dependent fluorescent protein-expressing AAV (AAV/DJ-hSyn-CreON/FlpON-ChR2-eYFP) was injected into the MRR of 3 vGluT2-Cre mice.*

F: *MRR vGluT2 cells labeled using intersectional viral tracing methods according to panel E.*

G: *The axon collaterals of MRR vGluT2 neurons that target the LHb also target memory formation-related hippocampus-projecting brain areas (including the MS-VDB) and valence processing-related subcortical regions (including the lateral LH, LPO, DR, PCG, VTA, and the IPN). Scale bar for F-G: 200 µm.*

H: *AAV2/5-EF1α-DIO-eYFP was injected into the MRR and AAV2/5-EF1α-DIO-mCherry was injected into the LHb of vGluT2-Cre mice bilaterally (n=2).*

I: *Injection site in the LHb and its vGluT2-positive fibers in the MRR. Scale bars: 200 µm.*

J: *vGluT2-positive LHb fibers (red) establish Homer-1 (white) positive synaptic contacts (white arrowheads) with vGluT2-positive MRR neurons (green). Scale bar: 10 µm.*
K: *vGluT2-positive MRR fibers (green) establish Homer-1 (white) positive synaptic contacts (white arrowheads) with vGluT2-positive LHb neurons (red). Scale bar: 5 µm.*
L: *AAV2/5-EF1α-DIO-eYFP was injected into the MRR of vGluT2-Cre mice (n=3).*
M: *A representative MS/VDB PV-positive neuron (red) is innervated by basket-like multiple synapses of vGluT2-positive MRR fibers (green), establishing Homer 1-positive (white) synaptic contacts (white arrowheads). Scale bar: 10 µm.*
N: *AAV2/5-EF1α-DIO-mCherry was injected into the MRR and FG into the bilateral hippocampi of vGluT2-Cre mice (n=2).*
O: *AAV-mCherry containing vGluT2-positive MRR terminals (red) establish several putative contacts (white arrowheads) with a FG-positive (green) septohippocampal PV-positive (blue) neuron. Scale bar: 10 µm.*
Published in (110).

Table 4. Stereological estimation of MRR vGluT2 neurons

	Mouse1	**Mouse2**	**Mouse3**	**Average**
Total counted vGluT2-positive neurons	8524	7014	4826	6788
Total counted TpH or/and vGluT3 positive neurons	5886	3362	3995	4414
vGluT2-positive neurons / TpH and-or vGluT3 positive neurons	1,45	2,09	1,21	1,58
All TpH and/or vGluT3 positive MRR neurons (94)				6067
Total MRR neurons (94)				47458
vGluT2-positive neurons in MRR				1,58*6067 = 9586
vGluT2-positive neurons ratios in MRR				**20,20%**

To investigate further the anatomical connection between the MRR and LHb, we performed double anterograde viral tracing by injecting a Cre-dependent eYFP-encoding virus into the MRR and a Cre-dependent mCherry-encoding virus into the LHb of vGluT2-Cre mice (Fig. 4H). We found that MRR vGluT2 neurons form basket-like synapses with LHb vGluT2 neurons (Fig. 4K). Furthermore, we also observed that LHb vGluT2 neurons densely innervate the MRR (Fig. 4I) and 39% (201/518 terminals from 2 mice) of LHb terminals make synaptic contacts with vGluT2-positive neurons in the

MRR (Fig. 4J). These results indicate an excitatory positive feedback loop between the vGluT2-neurons of MRR and LHb.

Fast and effective processing of negative experiences requires the immediate induction of memory acquisition, which necessitates a rapid change in the state of the MS/VDB-hippocampal system (111).

After viral labeling of LHb-projecting MRR vGluT2 neurons, we observed dense axonal labeling in the MS-VDB (Fig. 4G). Our fluorescence measurements revealed that at least 79% (497/626 terminals from 2 mice) of MRR vGluT2 axon terminals establish Homer-positive excitatory synaptic contacts on parvalbumin (PV) positive GABAergic cells (Fig. 4L-M). Furthermore, we found that at least 53% (35/66 cells from 2 mice) of PV-positive cells in the MS-VDB received at least one synaptic contact from MRR vGluT2 neurons. Using hippocampal injections of the retrograde tracer FluoroGold (FG), in combination with AAV2/5-EF1α-DIO-mCherry into the MRR of vGluT2-Cre mice, we found that MRR vGluT2 neurons directly innervate hippocampus-projecting PV neurons in MS-VDB (Fig. 4N-O). These experiments demonstrate that MRR vGluT2 neurons innervate PV neurons that are the pacemakers of memory acquisition–promoting hippocampal theta rhythm (112,113).

4.1.3. MRR vGluT2 neurons receive inputs from negative experience processing brain regions

To identify the brain areas that target MRR vGluT2 neurons via direct synaptic connections, we used mono-transsynaptic rabies tracing. We infected MRR vGluT2 neurons in vGluT2-Cre mice directly, with a Cre-dependent helper virus (encoding TVA, oG, and GFP proteins) and we injected a retrograde, glycoprotein-deleted mCherry-encoding rabies virus into the MRR of the same mice (Fig. 5A-B). Areas that play an essential role in valence- and negative-experience-processing, including the DR, VTA, LH, PAG, LDTg, LPO, and VP, showed a strong convergence onto MRR vGluT2 neurons (Fig. 5C-D). Areas related to encoding aversive memories, including the Mamillary nuclei (Mam), PFC, and nucleus incertus (NI), also sent projection onto MRR vGluT2 neurons (Fig. 5C-D). The LHb contained the most retrogradely labeled cells (Fig. 5D), further confirming the excitatory positive feedback loop between the MRR and LHb.

These results suggest that MRR vGluT2 neurons are at the center of processing negative experiences.

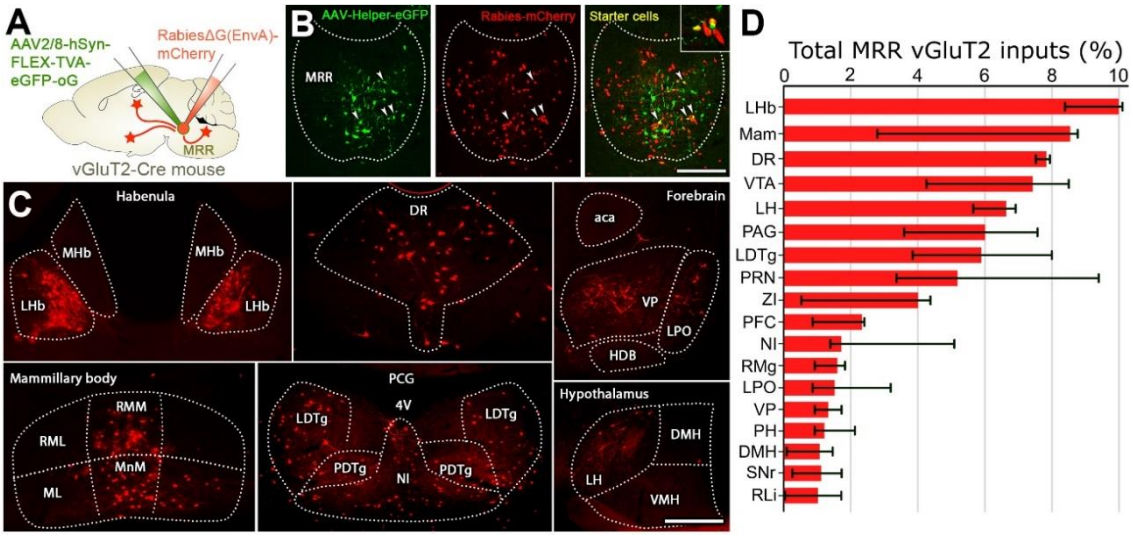

Figure 5. Monosynaptic inputs of MRR vGluT2 neurons

A: *A helper AAV2/8-hSyn-FLEX-TVA-eGFP-oG was injected into the MRR of vGluT2-Cre mice, followed by an injection of Rabies(ΔG)-EnvA-mCherry 4 weeks later (n=3 mice).*

B: *Injection site of helper (green) and rabies (red) viruses into the MRR of vGluT2-Cre mice. The inset shows some starter neurons expressing both viruses. Scale bar: 100 µm.*

C: *Representative fluorescent images show the retrogradely labeled monosynaptic inputs (red) of the MRR vGluT2 neurons. Scale bar: 100 µm.*

D: *Graph shows the ratio of neurons in brain areas that target the MRR vGluT2 neurons (medians and interquartile ranges). Abbreviations: PRN: pontine reticular nucleus, ZI: zona incerta, RMg: raphe magnus, PH: posterior hypothalamus, DMH: dorsomedial hypothalamus, SNr: substantia nigra pars reticularis, RLi: rostrolinear nucleus.*

Published in (110).

4.1.4. Stimulation of MRR vGluT2 neurons causes strongly aversive behavior

Our anatomical observations showed that MRR vGluT2 neurons are strongly linked to negative experience-related brain areas, therefore, we investigated how the stimulation of MRR vGluT2 neurons influences mouse behavior. Therefore, we conducted optogenetic in vivo behavioral experiments in mice, infecting their MRR vGluT2 neurons either with ChR2-encoding Cre-dependent AAV (AAV2/5-EF1α-DIO-ChR2-eYFP, “ChR2 mice”) or with only fluorescent protein-encoding AAV (AAV2/5-

EF1α-DIO-eYFP, “CTRL mice”). Then, we implanted an optic fiber over the MRR (Fig. 6A). After 5 days of handling, we conducted real-time place aversion (RTPA) and conditioned place aversion (CPA) tests on different days, where mice were placed into a box containing two different chambers with different environmental cues (Fig. 6A). On the habituation day, neither ChR2 mice nor CTRL mice showed a preference for either chamber of the double-chamber box (Fig. 6A-B). On the next day, all mice were again placed in the same double-chamber box, and the MRR of these mice received continuous light illumination when the mice entered one of the chambers (chamber selection was systematically randomized). In contrast to CTRL mice, ChR2 mice showed a strong, immediate real-time place aversion (RTPA) for the optic fiber stimulated chamber of the double-chamber box (Fig. 6B). On the next day, ChR2 mice, but not CTRL mice, showed a strong conditioned place aversion (CPA) of the previously stimulated chamber, indicating that they formed aversive contextual memories (Fig. 6B). These experiments revealed that stimulation of MRR vGluT2 neurons induced negative emotional valence in mice.

Following this experiment, we tested in the same mice whether the optogenetic activation of MRR vGluT2 neurons was sufficiently aversive to override motivated, goal-directed behavior. During an operant conditioning paradigm, food-restricted mice learned for 10 days that pressing a lever resulted in the delivery of a food pellet, and by the end of the training period, lever-pressing behavior had reached a stable maximum (Fig. 6C-D). On day 11, each lever press was paired with a short (5-second) light stimulation of MRR vGluT2 neurons (Fig. 6C). We found that ChR2 mice significantly reduced their lever-pressing behavior compared to the previous day, whereas lever pressing in CTRL mice remained unaffected (Fig. 6D). Moreover, the change in lever-pressing behavior was significantly different between the groups: ChR2 mice pressed the lever much less, while CTRL mice continued pressing at the same rate (Fig. 6E). These results indicate that activation of MRR vGluT2 neurons elicits a strongly aversive experience that is powerful enough to suppress reward-seeking behavior even in highly motivated mice.

4.1.5. MRR vGluT2 neurons are necessary for fear memory formation

The activation of MRR vGluT2 neurons is sufficient for encoding a negative experience in itself and they convey information to the negative experience processing related brain centers and memory formation-related brain areas as well. Therefore, we investigated, whether the activity of these neurons is necessary for the memory formation of a negative experience (e.g. for the well-researched fear memory formation). We injected Cre-dependent Archaerhodopsin (ArchT)-encoding AAV2/5-CAG-FLEX-ArchT-GFP ("ArchT mice") or control Cre-dependent AAV2/5-EF1α-DIO-eYFP ("CTRL-mice") into the MRR of vGluT2-Cre mice, and implanted an optic fiber over the MRR (Fig. 6F). After 5 days of handling, mice were tested in a cued fear conditioning paradigm. First, we placed mice into a new context "A" (CTXA), where they received three auditory tones, at the end of which they received foot shocks and light illuminations. Light delivery was precisely aligned to foot shocks (Fig. 6F). All mice displayed equally strong immediate reactions to foot shocks. In the following tests, mice received no more light illumination. On the next day, mice were placed into the same CTXA to test their contextual fear memories. We observed that CTRL mice expressed strong contextual freezing behavior as expected, whereas ArchT mice showed almost no freezing behavior in CTXA (Fig. 6F). On the next day, we placed mice into a completely different, neutral environment (context "B"), where ArchT mice showed significantly lower generalized fear compared to CTRL mice (Fig. 6F). Then, in the same neutral environment, we presented the mice with the auditory cue. CTRL mice showed very high levels of freezing as expected. In contrast, light inhibited ArchT mice showed significantly diminished freezing, indicating impaired cued fear memory formation (Fig. 6F). These results suggest that MRR vGluT2 neurons are necessary for the acquisition of both contextual and cue-related memories of negative experience.

DOI:10.14753/SE.2025.3206

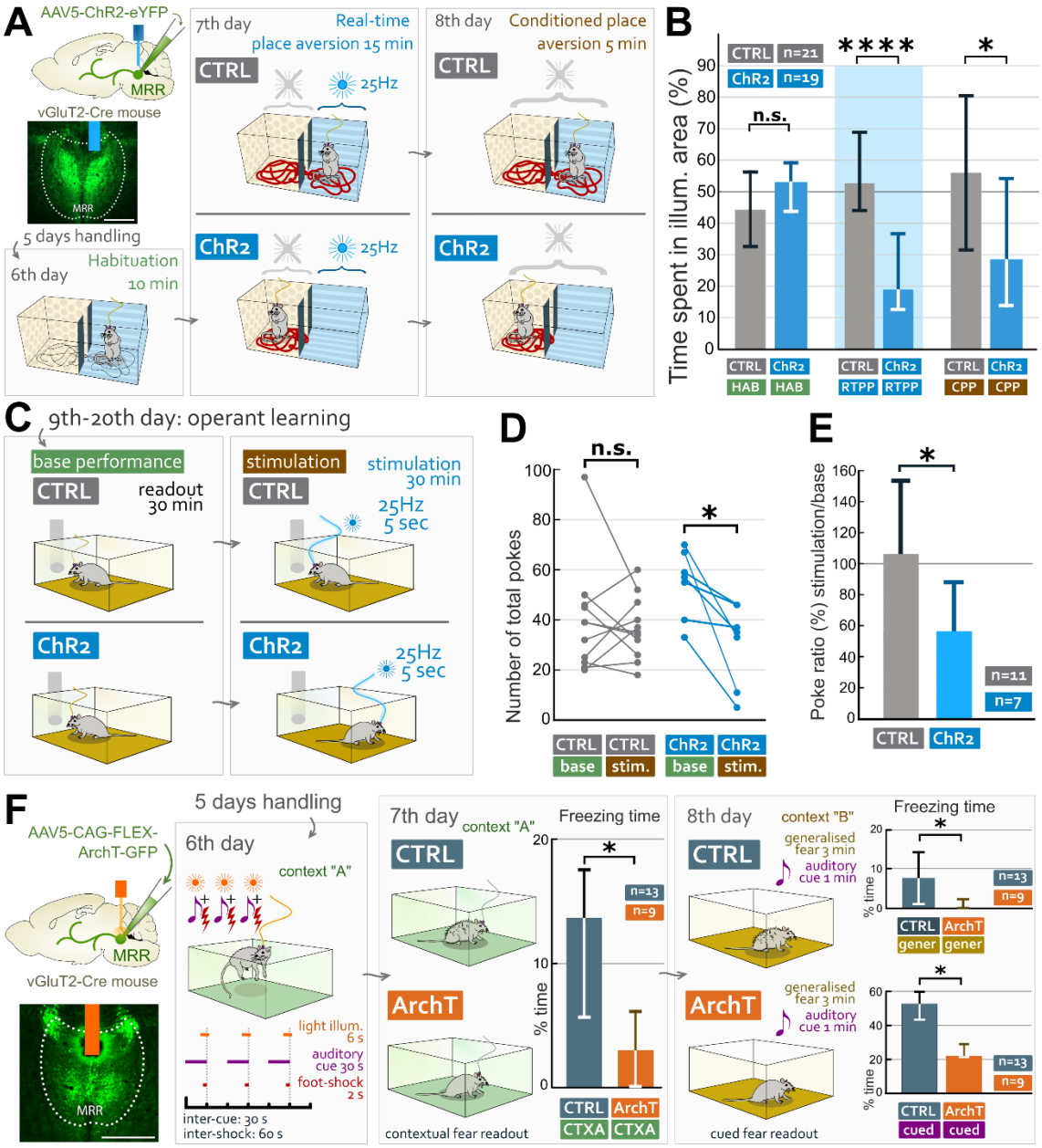

Figure 6. The activity of MRR vGluT2 neurons induces active avoidance and is necessary for fear memory formation

A: *After injecting ChR2-containing AAV ("ChR2 mice") or control (only eYFP-containing) Cre-dependent AAV ("CTRL mice") into the MRR of vGluT2-Cre mice, we implanted an optic fiber over the MRR. Image represents an injection site in MRR and the position of the optic fiber (blue). Scale bar: 500 µm. After 5 days of handling, mice were habituated to a box with two chambers. On day 7, mice received 25 Hz light illumination (15 mW, 10 ms pulse onset) in one of the chambers of the box. ChR2 mice showed immediate, significant real-time place aversion (RTPA) of the illuminated area. On day 8, no light was presented, but ChR2 mice displayed a significant*

conditioned place aversion (CPA), suggesting that the activity of MRR vGluT2 neurons can directly induce real-time and learned active contextual avoidance.

B: *The graph shows that, compared to non-stimulated CTRL mice, ChR2 mice spent significantly less time in the chamber associated with the MRR stimulation, showing both RTPA and CPA (medians and interquartile ranges).*

C: *Between days 9 and 21, mice were food-restricted and learned to nose-poke for reward pellets. On day 22, mice received 5-second-long 25Hz light stimulation on nose-pokes. Compared with base performance (on day 21), ChR2 mice performed significantly fewer nose-pokes when nose-pokes were paired with laser stimulation (on day 22).*

D: *The total number of nose-pokes for rewards during the base (day21) and stimulation performance (day22) in the operant conditioning task.*

E: *Nose-poke ratios of stimulation/base performance in the operant conditioning task (mean and SD).*

F: *Design of cued fear conditioning experiments with optogenetic inhibition of MRR vGluT2 neurons. Fluorescent image represents one of the injection sites to label MRR vGluT2 neurons, and the orange area represents the position of the optic fiber. Scale bar: 500 µm. After 5 days of handling, light illumination of MRR was switched on precisely during foot shocks that mice received at the end of the auditory cue presentation on day 6. On days 7 and 8, mice received no more light. On day 7, contextual freezing behavior (CTXA) in ArchT mice in the same environment was almost completely diminished compared with CTRL mice. On day 8, ArchT mice showed significantly less generalized fear (gener) and cued fear (cued) in a novel environment compared with CTRL mice (medians and interquartile ranges).*

For statistical details, see Table 5.

Published in (110).

4.2. Inhibitory innervation to the LHb from the Brainstem

4.2.1. A novel LHb-innervating pontine GABAergic nucleus: the SVTg

The LHb relies on inhibition to maintain a balanced emotional state and decision-making. However, brainstem-derived inhibitory input to the LHb was previously unknown, and overall, the LHb was known to receive minimal purely inhibitory (GABAergic) inputs. Therefore, we investigated all GABAergic neuronal inputs of the LHb by injecting a fluorescent protein-expressing Cre-dependent retrogradely spreading AAV (AAVretro-hSyn-FLEX-GCaMP8m) into the LHb of vGAT-Cre mice (Fig. 7A-B). This experiment revealed a previously unrecognized nucleus under the fourth ventricle in the brainstem pontine central grey, retrogradely labeled from the LHb (Fig. 7C). We named it the subventricular tegmental nucleus or SVTg (Fig. 7C). Our quantification showed that 15% of the LHb inhibitory inputs originated from SVTg (Fig. 7D-E), making SVTg the largest purely GABAergic input of the LHb, while all GABAergic cells of the EPN and VTA co-express and co-release glutamate (67,68). Using immunohistochemistry on coronal brain slices, we found that SVTg→LHb GABAergic neurons are clearly separated from adjacent choline acetyltransferase (ChAT)-positive laterodorsal tegmentum (LDTg), tyrosine hydroxylase (TH)-positive locus coeruleus (LC) and tryptophan hydroxylase (TpH)-positive dorsal raphe (DR) neuronal populations (Fig. 7F-G). We found that the SVTg extends far beyond the adjacent LDTg and dorsal tegmentum (DTg) both rostrally and caudally.

Our anterograde viral labeling revealed that SVTg neurons densely innervate the LHb (Fig. 7I). We also investigated eYFP-labeled axonal terminals of SVTg in vGAT-Cre mice (injected with AAV2/5-EF1α-DIO-eYFP into the SVTg) and found that 92% of them (573/620 terminals from 4 mice) were positive for vGAT, but not for vGluT2 (35/576 terminals from 2 mice), nor vGluT3 (2/168 terminals from 2 mice), nor vAChT (0/218 terminals from 2 mice) in the LHb (Fig. 7J).

DOI:10.14753/SE.2025.3206

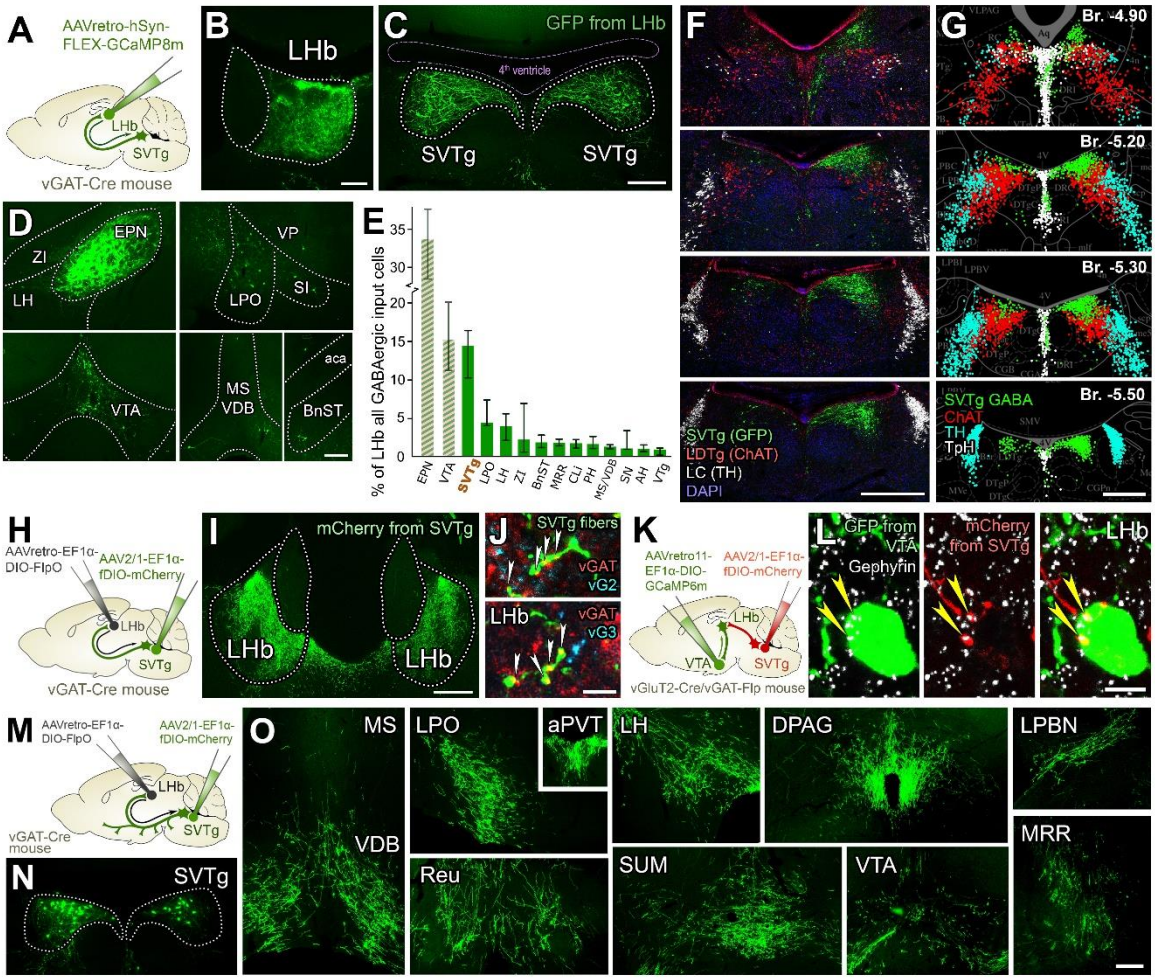

Figure 7. Localization and innervation outputs of the SVTg

A: *Cre-dependent GCaMP8m(GFP)-expressing retrograde AAV was injected into the LHb of vGAT-Cre mice bilaterally (n=4).*

B: *Representative fluorescent images show the injection site in the LHb. Scale bar: 200 µm.*

C: *Fluorescent image shows a large population of neurons, the SVTg labeled from the LHb under the fourth ventricle. Scale bar: 200 µm.*

D: *Fluorescent images show LHb retrogradely labeled inhibitory inputs in the entopeduncular nucleus (EPN), lateral hypothalamus (LH), zona incerta (ZI), ventral tegmental area (VTA), bed nucleus of the stria terminalis (BnST), medial septum/ vertical limb 1 of diagonal band of Broca (MS/VDB), lateral preoptic area (LPO), substantia innominata (SI) and ventral pallidum (VP) in vGAT-Cre mice (n=4 mice). Scale bar: 200 µm.*

E: *Graph shows the percentage of all GABAergic input cells of the LHb from 4 mice. Our measurements showed that the SVTg is the largest purely GABAergic input of the LHb (medians and interquartile ranges).*

F: *Confocal-laser scanning images show that virally labeled SVTg GABAergic neurons (green) are separated from LDTg ChAT-positive (red) and LC TH-positive (white) neurons. Scale bar: 500 μm.*

G: *Reconstructed location of distinct neurons of different pontine nuclei on coronal sections from original slices taken from Br.-4.90 mm, Br.-5.20 mm, Br.-5.30 mm, and Br.-5.50 mm (from n=3 mice). SVTg neurons (green), ChAT positive neurons (red), TH positive neurons (cyan), and TpH positive neurons (white). Scale bar: 500 μm.*

H-I: *A Cre-dependent Flippase-expressing retrograde AAV (colorless) was injected into the LHb, additionally a Flippase-dependent mCherry expressing AAV was injected into the SVTg of vGAT-Cre mice (n=4). Then, mCherry-labeling revealed (I) abundant SVTg innervation of the LHb (green). Scale bar: 200 μm.*

J: *Confocal-laser scanning images show that virally labeled SVTg fibers (green, white arrows) in the LHb are only positive for vGAT (red), but not for vGluT2 (vG2, upper image, cyan) nor vGluT3 (vG3, bottom image, cyan). Scale bar: 5 μm.*

K: *Cre-dependent GCaMP6m(GFP) expressing retrograde AAV was injected into the VTA, additionally a Flippase-dependent mCherry expressing AAV was injected into the SVTg of vGluT2-Cre/vGAT-Flp double transgenic mice (n=3).*

L: *SVTg fibers (red) establish gephyrin (white) positive putative synaptic contacts (yellow arrowheads) with the soma of VTA-projecting glutamatergic LHb cells (green). Scale bar: 10 μm.*

M: *Cre-dependent Flp-expressing colorless retrograde AAV (AAVretro-EF1α-DIO-FlpO) was injected into the LHb, and Flp-dependent fluorescent protein-expressing AAV (AAV2/1-EF1α-fDIO-mCherry) was injected into the SVTg of 4 vGAT-Cre mice.*

N: *SVTg GABAergic neurons labeled using intersectional viral tracing methods according to panel M.*

O: *The axon collaterals of SVTg neurons that target the LHb also target valence processing-related subcortical regions [including the lateral preoptic area (LPO), the anterior part of the paraventricular thalamus (aPVT), the lateral hypothalamus (LH), the dorsal periaqueductal grey (DPAG), the lateral parabrachial nucleus (LPBN), the median raphe region (MRR), and the VTA] and memory formation-related hippocampus-projecting brain areas [including the vertical limb of the diagonal band of Broca (VDB), the nucleus reuniens thalami (Reu), and supramammillary nucleus (SUM)]. Scale bar for N-O: 200 μm.*

Published in (114).

LHb neurons broadcast the negative valence signal to the VTA. To investigate whether the VTA-projecting LHb (LHb→VTA) neurons are directly inhibited by the SVTg→LHb neurons, we used a double transgenic vGluT2-Cre/vGAT-Flp mouse. We infected LHb→VTA neurons retrogradely from the VTA using a Cre-dependent AAVretro11-EF1α-DIO-GCaMP6m and labeled the SVTg neurons anterogradely from the SVTg using an Flp-dependent AAV2/1-EF1α-fDIO-mCherry (Fig. 7K). We found that the SVTg neurons established gephyrin-positive putative synaptic contacts with the somata and dendrites of LHb→VTA neurons (Fig. 7L). Our measurement showed that at least 69% (20/29) of VTA-projecting cells receive at least one synaptic contact (on average 4.55) from SVTg neurons.

To investigate the axonal collaterals of SVTg→LHb neurons we performed anterograde intersectional viral tract tracing as described above (Fig. 7M-N). This revealed that SVTg→LHb neurons also targeted other memory formation-related brain areas (VDB, Reu, SUM) and other valence processing-related subcortical regions (LPO, aPVT, LH, DPAG, LPBN, MRR, VTA) (Fig. 7O).

4.2.2. Stimulation of SVTg induces positive valence and reward-seeking behavior

LHb inhibition is known to induce a rewarding experience, therefore, we tested the effect of optogenetic stimulation of the SVTg. To perform this, we injected a Cre-dependent AAVretro-EF1α-DIO-ChR2-mCherry expressing virus ("ChR2 mice") or a control mCherry containing Cre-dependent AAVretro-EF1α-DIO-mCherry virus ("CTRL mice") into the LHb of vGAT-Cre mice, labeling the SVTg→LHb neurons retrogradely. Then, we implanted optic fibers over the SVTg bilaterally (Fig. 8A). After handling, we conducted real-time place preference (RTPP) and contextual place preference (CPP) tests on different days (Fig. 8B). On the habituation day, mice showed no preference for either chamber of the double-chamber box (Fig. 8C). On the next day, all mice were again placed in the same double-chamber box, and the SVTg of these mice received continuous light exposure when the mice entered one of the chambers (Fig. 8B). In contrast to CTRL mice, ChR2 mice showed a strong, immediate real-time place preference (RTPP) for the optic fiber stimulated chamber of the double-chamber box (Fig. 8C-D). On the following day, mice were placed back into the dual-chamber box without light stimulation. ChR2 mice, but not CTRL mice displayed strong conditioned

place preference (CPP) towards the previously stimulated chamber of the box (Fig. 8C-D).

To prove that the SVTg fibers targeting the LHb are directly responsible for inducing place preference behavior, we performed a similar experiment but stimulated the SVTg fibers in the LHb only (Fig. 8E). We injected anterograde Cre-dependent AAV2/5-EF1α-DIO-ChR2-eYFP ("ChR2 mice") or AAV2/5-EF1α-DIO-eYFP ("CTRL mice") into the SVTg of vGAT-Cre mice (Fig. 8E). We then implanted optic fibers above the LHb (Fig. 8E) and performed the same RTPP and CPP experiments as above. Again, we found that, in contrast to CTRL mice, ChR2 mice showed strong real-time and conditioned place preference towards the stimulated chamber of the box (Fig. 8F).

To test, whether mice actively seek SVTg stimulation, we conducted an optogenetic self-stimulation experiment. The SVTg→LHb neurons were infected retrogradely from the LHb of vGAT-Cre mice, either with AAVretro-EF1α-DIO-ChR2-mCherry ("ChR2 mice") or with AAVretro-EF1α-DIO-mCherry ("CTRL mice") (Fig. 8G). We then implanted optic fibers above the SVTg (Fig. 8G). We conducted an operant conditioning task with 2 nose-poke holes on mice that were food-restricted (Fig. 8H). Mice received a short, 2-second-long optogenetic light illumination only, when they poked their noses into the predefined, light-illuminated (ILLUM) holes (Fig. 8H). We used 20 Hz illumination during the first 3 days, and 40 Hz for another 7 days (Fig. 8I). We found that ChR2 mice poked their noses into the predefined hole (ILLUM, where their SVTg was illuminated) significantly more than CTRL mice, so much so that by the last day of training (day 10), ChR2 mice poked their noses into the predefined hole more than 8 times more often than CTRL mice (Fig. 8I). Finally, we tested the memory of the preference of these mice in the absence of light exposure on a separate day. We found that the performance of the ChR2 mice decreased but they still preferred the predefined (ILLUM) hole significantly more than the CTRL mice (Fig. 8I-J). These experiments demonstrate that activation of SVTg encodes positive valence and reward-seeking behavior in mice.

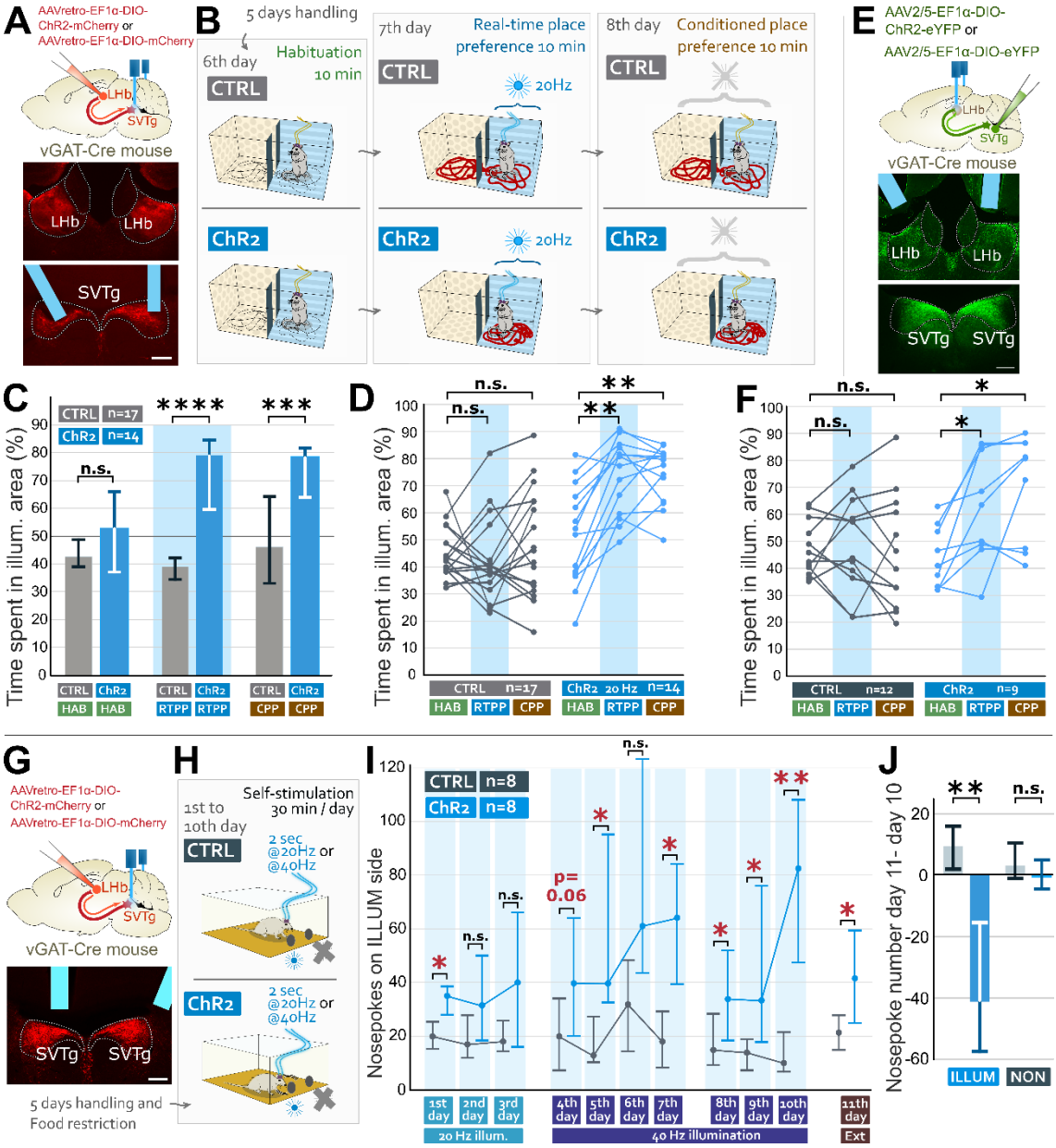

Figure 8. Stimulation of SVTg induces positive experience in mice

A: *We injected Cre-dependent retrograde AAVs that either expressed ChR2 (ChR2 mice) or did not express ChR2 (CTRL mice) into the LHb of vGAT-Cre mice and implanted optic fibers over the SVTg, bilaterally. Fluorescent images show the injection sites in the LHb and the position of the optic fibers (blue) and retrograde labeling of the SVTg neurons (red). Scale bar: 200µm.*

B: *After handling, mice were habituated (HAB) to a box with two chambers. On day 7, mice received 20 Hz optical fiber illumination (8-10mW, 10ms pulse onset) in one of the chambers to test real-time place preference (RTPP). On day 8, the conditioned place preference (CPP) of mice was tested in the same box without light illumination.*

C: *The graph shows that, compared to non-stimulated CTRL mice, ChR2 mice spent significantly more time in the chamber associated with the SVTg-stimulation, showing both RTPP and CPP (medians and interquartile ranges).*

D: *Chamber preference of individual mice during days 6 (HAB), 7 (RTPP), and 8 (CPP) of the experiment.*

E: *We bilaterally injected Cre-dependent anterograde AAVs with (ChR2 mice) or without the expression of ChR2 (CTRL mice) into the SVTg of vGAT-Cre mice and optic fibers were implanted over the LHb, bilaterally. The fluorescent images show the injection site in the SVTg and the position of the optic fibers (blue) over the LHb. Scale bar: 200µm. The same behavioral experiment was performed as described in (B) but here we illuminated the fibers of the SVTg in the LHb.*

F: *Chamber preference of individual mice during days 6 (HAB), 7 (RTPP), and 8 (CPP) of the experiment.*

G: *We injected Cre-dependent retrograde AAVs that either expressed ChR2 (ChR2 mice) or did not express ChR2 (CTRL mice) into the LHb of vGAT-Cre mice and implanted optic fibers over the SVTg, bilaterally. Fluorescent image shows the position of the optic fibers (blue) and retrograde labeling of the SVTg neurons (red). Scale bar: 200µm.*

H: *After handling, food-restricted CTRL and ChR2 mice were placed into a chamber containing two nose-poke holes. Tests lasted for ten days, 30 minutes each day. Mice received 2-second-long 20 Hz and later 40 Hz light illumination when they inserted their noses into the predefined hole (ILLUM side).*

I: *The graphs show that the ChR2 mice stuck their noses significantly more into the hole, where they received optic fiber illumination (ILLUM side), compared to CTRL mice on several different days. Self-stimulation at 40 Hz seemed to be slightly more effective. Experimental days were consecutive days except for experimental day 8 which started 2 weeks after day 7 (medians and interquartile ranges).*

J: *The graph shows the differences in the number of nose-pokes between days 11 and 10 on the illuminated (ILLUM) and non-illuminated (NON) holes (medians and interquartile ranges).*

For statistical details, see Table 5.

Published in (114).

4.2.3. Activity of SVTg is required for balanced assessment of valence

Using optogenetic inhibition in behaving mice *in vivo*, we investigated whether the continuous activity of the SVTg is required for the maintenance of a balanced valence circuit. We injected a Cre-dependent AAVretro-hSyn-SIO-stGtACR2-FusionRed

expressing virus (“stGtACR2 mice”) or a control mCherry containing Cre-dependent AAVretro-EF1α-DIO-mCherry virus (“CTRL mice”) into the LHb of vGAT-Cre mice, labeling the SVTg→LHb neurons retrogradely and then we implanted optic fibers over the SVTg bilaterally (Fig. 9A). After handling, we performed RTPA and CPA tests, on separate days (Fig. 9B). On the first experimental day, mice were placed into a double-chamber box for habituation to the new environment, where neither CTRL nor stGtACR2 mice showed any place preference (Fig. 9C). On the next day, mice were placed back into the same box and received continuous SVTg illumination only in one of the chambers (Fig. 9B). In contrast to CTRL mice, stGtACR2 mice showed a significant, immediate RTPA for the SVTg-inhibited-chamber (Fig. 9C-D). On the following day, all mice were placed back into the same dual chamber box without light illumination, and we tested their conditioned place aversion (CPA) (Fig. 9B). In contrast to CTRL mice, stGtACR2 mice showed significant CPA in the chamber, where their SVTg neurons were previously inhibited (Fig. 9C-D). This suggests that the SVTg has a baseline neuronal activity that is necessary to maintain a healthy valence detection and motivational state during spatial exploration.

Next, we tested how mice coped with fear without the activity of the SVTg neurons. Here, the above-mentioned, same stGtACR2 and CTRL mice were investigated during a contextual fear conditioning experiment (Fig. 9E). All mice received four aversive foot-shocks in context A (CTXA), precisely aligned with a short, 6-second-long optogenetic illumination of the SVTg neurons (Fig. 9E-F). During the conditioning, no difference was found in fear responses between CTRL and stGtACR2 mice (Fig. 9F). On the next day, we placed mice back into CTXA and found that, unlike CTRL mice, stGtACR2 mice showed a significant, more than two times higher contextual fear response (Fig. 9G). Later, we placed mice into a novel context (CTXB) to examine their generalized fear responses (Fig. 9E), and we found that it was still significantly higher in stGtACR2 mice (Fig. 9G). These data show that the SVTg is essential for controlling the strength of fear memory formation and actively preventing abnormal overgeneralization.

DOI:10.14753/SE.2025.3206

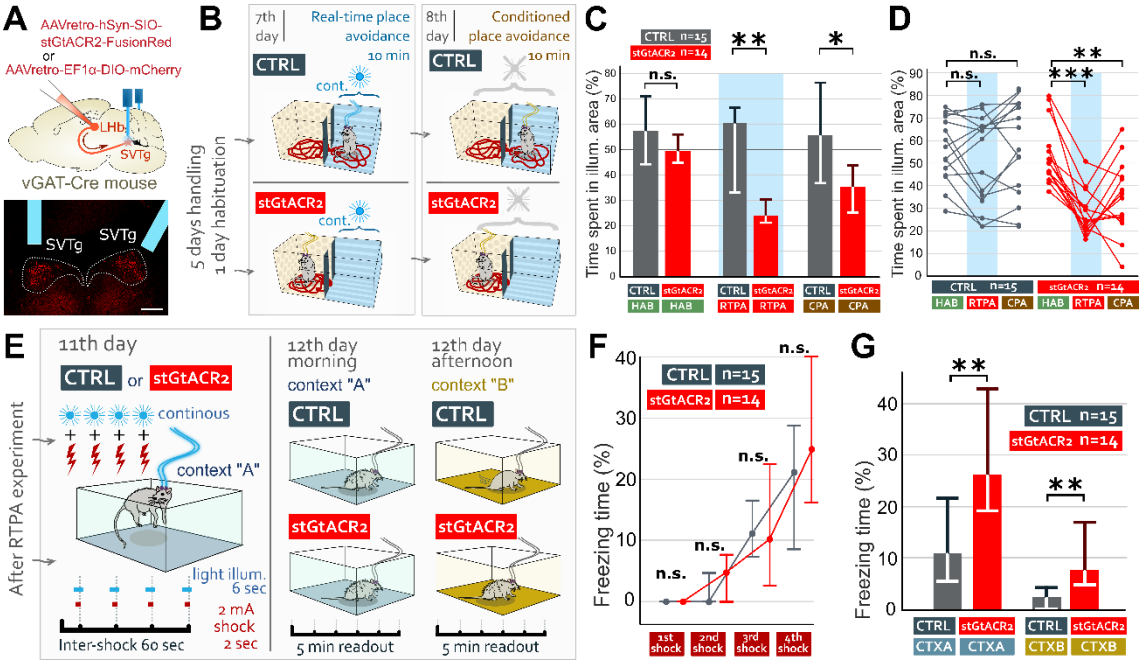

Figure 9. Inhibition of SVTg neurons induces negative experience in mice

A: *We injected Cre-dependent retrograde AAVs that either expressed the inhibitory opsin stGtACR2 (stGtACR2 mice) or did not express the stGtACR2 (CTRL mice) into the LHb of vGAT-Cre mice. Both viruses contained a reporter protein. Then, we implanted optic fibers over the SVTg, bilaterally. The fluorescent image shows an example position of the optic fibers (blue) and the retrogradely labeled SVTg neurons (red). Scale bar: 200µm.*

B: *After 5 days of handling, mice were habituated (HAB) to a dual-chamber box. On day 7, mice received continuous optic fiber light illumination for 10 min, to test their potential real-time place avoidance (RTPA). On day 8, mice were placed back into the same box, but without light illumination, to test their potential conditioned place avoidance (CPA).*

C: *Graphs show that mice did not prefer any of the chambers during habituation (HAB). stGtACR2, but not CTRL mice demonstrated significant RTPA and CPA (medians and interquartile ranges).*

D: *Pairwise comparisons also show that, unlike CTRL mice, stGtACR2 mice avoided the chamber significantly more in which their SVTg were inhibited.*

E: *After RTPA and CPA tests, CTRL and stGtACR2 mice received four foot shocks (2 mA, 2 sec) precisely aligned with optic fiber illumination (8-10 mW, 6 sec) of the SVTg in context A (CTXA). On the next day, mice were placed back into CTXA and then into a different context B (CTXB), while their fear behaviors (freezing) were recorded.*

F: *Graph shows the changes in behavioral freezing after the foot shocks for the CTRL and the stGtACR2 mice (medians and interquartile ranges).*

G: *Graphs demonstrate that the SVTg inhibition (in stGtACR2 mice) during negative experiences significantly increases fear responses (freezing time) in both CTXA and CTXB (medians and interquartile ranges).*
For statistical details see Table 5.
Published in (114).

4.2.4. SVTg neurons receive inputs from valence and salience-processing brain areas

To identify the brain areas that regulate the SVTg neurons via direct synaptic connections, we used mono-transsynaptic rabies tracing. We infected SVTg GABAergic neurons in vGAT-Cre mice directly, with a Cre-dependent helper virus (encoding TVA, oG and GFP proteins) and we injected a retrograde, glycoprotein-deleted mCherry-encoding rabies virus into the LHb of the same mice (Fig. 10A-B). We found that most of the inputs are received from adjacent reticular formation areas (pontine (PRN), mesencephalic (mRT) and gigantocellular reticular formation (Gi)) and key brain areas encoding valence, motivation, and aversion targeted the SVTg→LHb neurons mono-synaptically, including the MRR, IPN, ZI, LHb, DR and LDTg (Fig. 10C-D). Moreover, we found that higher-order associational cortical areas, the orbitofrontal cortex (OFC), the anterior cingulate cortex (ACC), and other PFC regions showed a strong convergence onto SVTg→LHb neurons (Fig. 10C-D).

Rabies labeling revealed that SVTg neurons are targeted by the MRR, which plays a fundamental role in aversive behavior (89,110). Therefore, we performed double tracing experiment to investigate this connection further by injecting a fluorescent protein-expressing Cre-dependent retrogradely spreading AAV (AAVretro-hSyn-FLEX-GCaMP8m) into the LHb and an anterograde Cre-OFF AAV2/9-EF1α-DO-ChR2-mCherry (that expressed mCherry only in neurons that did not express Cre) into the MRR of vGAT-Cre mice (Fig. 10E). We found that MRR non-GABAergic (possibly the vGluT2-positive glutamatergic) cells densely innervate the SVTg region (Fig. 10F). We found that at least 43% (20/47 cells from 4 mice) of SVTg neurons received, on average 2 or 3 homer-1 positive putative synapses (51 total) from the MRR (Fig10. G).

Because we found that the reward prediction and motivation encoding OFC directly targets SVTg neurons, we investigated this neuronal connection further. We performed a double tracing experiment by injecting an AAVretro-hSyn-FLEX-GCaMP8m into the LHb and an anterograde Cre-OFF AAV2/9-EF1α-DO-ChR2-

mCherry (labeling the non-GABAergic pyramidal cells) into the OFC of vGAT-Cre mice (Fig. 10H-I). We found that OFC pyramidal cells densely innervate the pontine SVTg (Fig. 10J) and form putative excitatory, homer-1 positive synaptic contacts with SVTg neurons (Fig. 10K). Our anatomical analysis revealed that at least 69% (40/58 cells from 4 mice) of SVTg neurons received, on average, about 4 to 5 synapses (176 total) from the OFC (Fig. 10K). These experiments revealed that both subcortical and higher-order cortical regions, conveying different types of information, converge onto SVTg neurons.

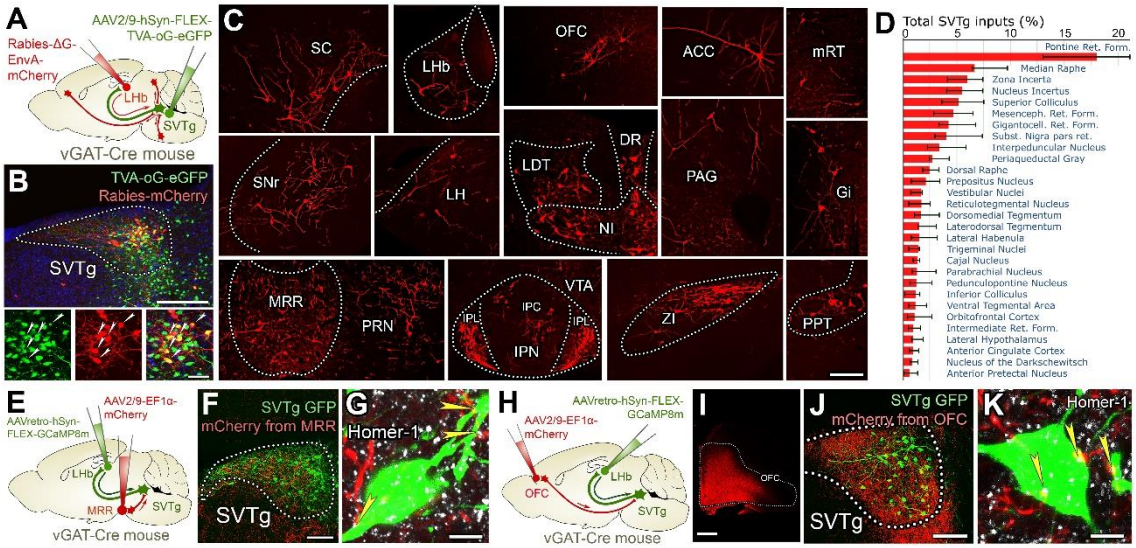

Figure 10. Monosynaptic inputs of SVTg neurons

A: *Cre-dependent, avian receptor-expressing "helper" AAVs were injected into SVTg, then 5 weeks later, avian receptor-dependent, mCherry-expressing, monosynaptically-restricted transsynaptic Rabies viruses were injected into the LHb of vGAT-Cre mice (n=5).*

B: *Fluorescent images show that yellow (white arrows) "starter" cells [that express both the helper (green) and rabies (red) virus products] are in SVTg. Scale bar: 200 µm (top), 20 µm (bottom).*

C: *Representative fluorescent images show the retrogradely labeled monosynaptic inputs (red) of SVTg neurons. Scale bar: 200 µm.*

D: *Graph shows the ratio of neurons in brain areas from n=5 mice that target the GABAergic neurons in SVTg (medians and interquartile ranges).*

E: *Retrograde labeling of GABAergic SVTg→LHb neurons was combined with the anterograde viral labeling of the non-GABAergic neurons (using AAV2/9-EF1α-DO-ChR2-mCherry virus that can only be expressed in non-Cre neurons) from the MRR in vGAT-Cre mice (n=4).*

F: *Images show that MRR (red, putative glutamatergic) fibers innervate SVTg. Scale bar: 100 µm.*

G: *MRR establishes homer-1 (white) positive synaptic contacts (yellow arrowheads) with SVTg neurons (green). Scale bar: 5 µm.*

H: *Retrograde labeling of SVTg GABAergic neurons from the LHb was combined with the anterograde viral labeling of the non-GABAergic neurons (using the AAV2/9-EF1α-DO-ChR2-mCherry virus that can only be expressed in non-Cre neurons) from the OFC in vGAT-Cre mice (n=4).*

I: *Fluorescent image shows the injection site in the OFC. Scale bar: 200 µm.*

J-K: *Image shows that OFC fibers (red) innervate SVTg and establish homer-1 (white) positive synaptic contacts (yellow arrowheads) with GFP-labeled SVTg neurons (green). Scale bars: 100 µm and 5 µm.*

Published in (114).

4.2.5. Typical molecular features of SVTg neurons

To identify SVTg neurons in different species without viral labeling, we investigated, which of its proteins could be used to label SVTg neurons selectively in different species. In collaboration, we examined the whole mRNA expression profile of SVTg neurons using single-cell mRNA sequencing and found that SVTg neurons specifically express some unique proteins that are rarely found in the brain. The presence of these proteins in SVTg neurons was further investigated and validated by immunohistochemistry. We found that the special AT-rich sequence-binding protein-1 (Satb1) transcription factor was highly selectively and specifically found in SVTg neurons (Fig. 11A-B). Our measurement showed that 96% (352/366 cells from 2 mice) of virally labeled SVTg→LHb neurons were positive for Satb1 (Fig. 11A) and virtually all (1553/1589 cells from 3 mice) Satb1 positive cells in the PCG were GABAergic in vGAT/ZsGreen transgenic mice (Fig. 11B). Moreover, we found that additional SVTg cell-specific markers were the transcription factor paired box protein 6 (Pax6) (Fig. 11C), the reelin (Reln) glycoprotein (Fig. 11D), and the T-type calcium ion channel Cav3.1 (Fig. 11E). Our measurement showed that 87% (287/331 cells from 2 mice) of virally labeled SVTg→LHb neurons were positive for Pax6, 95.5% (341/357 cells from 3 mice) of virally labeled SVTg→LHb neurons were positive for Reln and 94% (282/299 cells from 2 mice) of virally labeled SVTg→LHb neurons were positive for Cav3.1. We also

found that 81% (1123/1379 cells from 3 mice) of SVTg→LHb neurons were positive for Satb1, Pax6, and Reln simultaneously (Fig. 11F). Our immunostaining experiment revealed that the Satb1 staining and virally labeled SVTg→LHb neurons were completely and perfectly overlapped at the full rostro-caudal extent of the nucleus (Fig. 11G). These experiments suggest that the Satb1, Pax6, and Reln are selective markers of SVTg neurons, and especially the Satb1 can be used as a highly selective marker to identify SVTg in the pontine brainstem.

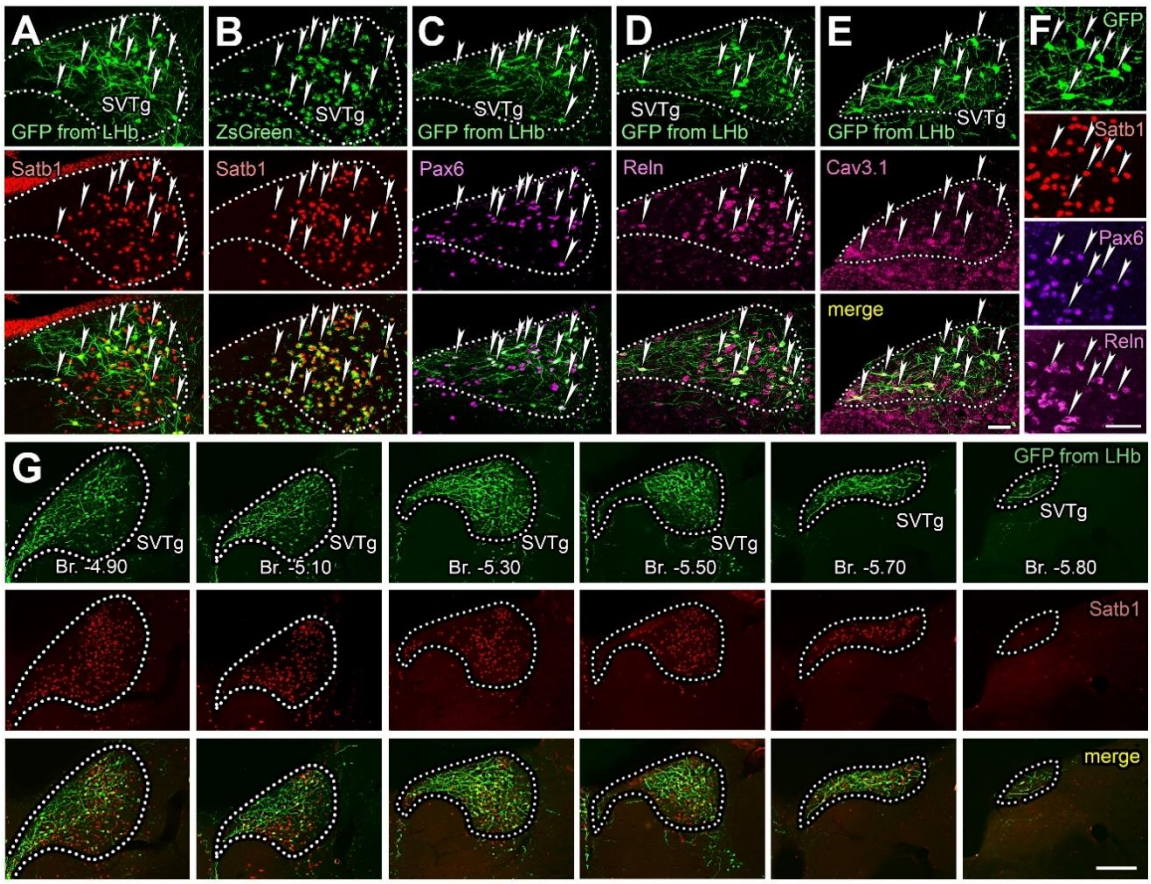

Figure 11. SVTg neurons are positive for Satb1, Pax6, and reelin

A: *Confocal laser-scanning images show that GFP-expressing SVTg neurons that were retrogradely labeled from the LHb (green, white arrowheads) strongly express Satb1 (red).*

B: *Images show that virtually all Satb1 positive neurons (red) were also positive for ZsGreen (green) in 3 vGAT/ZsGreen mice, indicating that Satb1 neurons are GABAergic in SVTg.*

C-E: *Images show that GFP-expressing SVTg neurons that were retrogradely labeled from the LHb (green, white arrowheads) strongly express Pax6 (C, purple), Reln (D, pink), and Cav3.1 (E, pink). Scale bar for A-E: 50 μm.*

F: *Confocal-laser-scanning images show that GFP-expressing SVTg neurons that were retrogradely labeled from the LHb (green, white arrowheads) simultaneously express Satb1 (red), Pax6 (purple) and Reln (pink). Scale bar: 50 μm.*
G: *Fluorescent images show that GFP-expressing SVTg neurons that were retrogradely labeled from the LHb (green) strongly express Satb1 (red) at the full-rostrocaudal extent (from Br. -4.90 mm to Br. -5.80 mm) of SVTg nucleus. Virtually all virally infected SVTg neurons (green) are Satb1 (red) positive (merged images). Scale bar: 200 μm.*
Published in (114).

4.2.6. SVTg in rodents, primates, and the human brain

The pontine brainstem is thought to be evolutionarily ancient and well-conserved, so its neuron populations are likely to be present or even more evolved in most mammalian brains (83). Because we found that Satb1 nuclear protein expression is highly specific for mouse SVTg neurons in the brainstem (Fig. 11G) Satb1 DAB-Ni precipitation-based immunohistochemistry was used to localize the SVTg in the rat (Wistar rat), rhesus monkey (*Macaca mulatta*), and human pontine brainstem.

In the rat, we found the Satb1-positive neurons in virtually the same location as in the mouse (Fig. 12A). In elder macaque and human brains, noradrenergic (LC) and serotonergic DR neurons contain neuromelanin, allowing these cells to be localized in the brainstem without specific staining. In three macaque brains, we found Satb1-positive neurons just below the fourth ventricle, between LC and DR neurons, and above the immunostained LDTg cholinergic neurons (Fig. 12B-G). In two human subjects, Satb1-positive neurons were localized just below the fourth ventricle (less than 300 μm), between the LC and DR neurons, at a similar location as in the macaque brain (Fig. 12H-O). We found no Satb1-like staining in the negative control (CTRL-staining) sections without primary antibodies (Fig. 12B, E, H, J, L, N). These experiments suggest that SVTg is an evolutionarily well-conserved nucleus in the pontine brainstem that can be found in mice, rats, monkeys, and in the human brain.

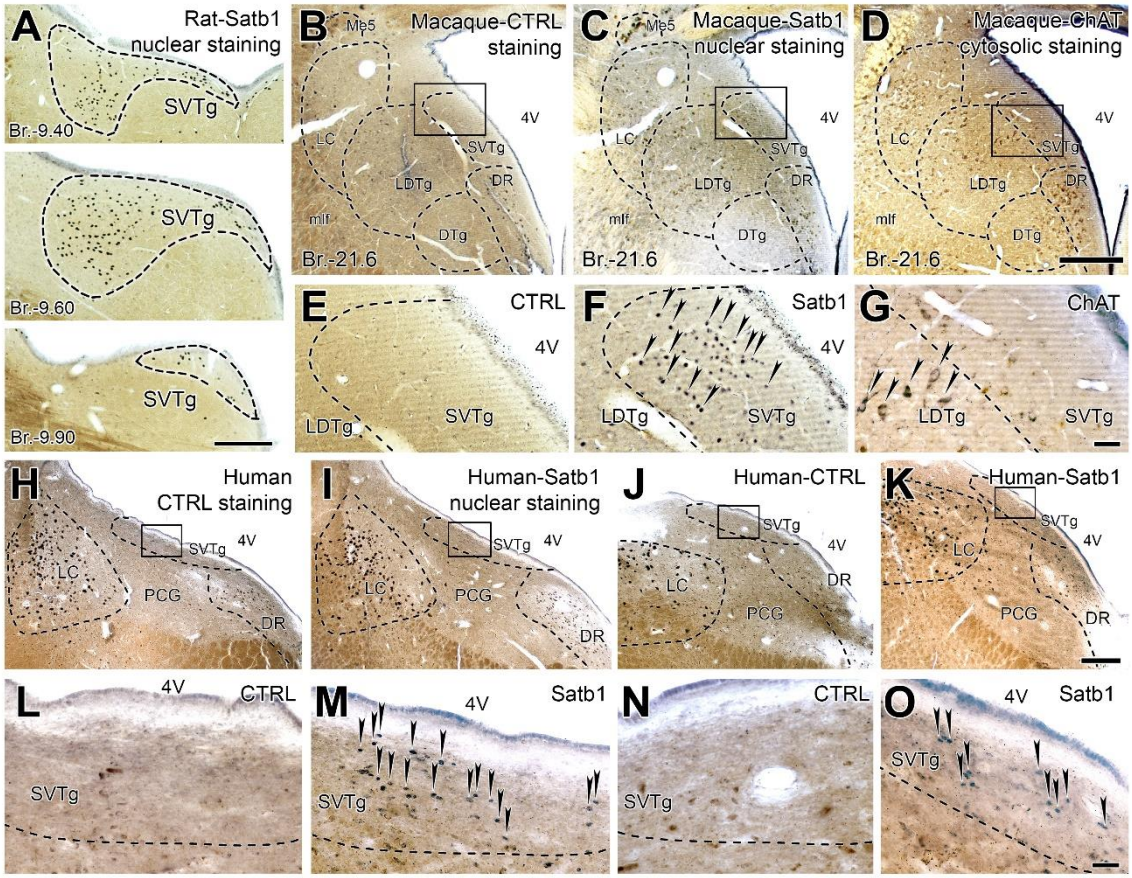

Figure 12. SVTg nucleus identified in rat, monkey, and human pontine brainstem

A: *Light microscopic images show Satb1-positive SVTg neurons (black nuclear DAB-Ni staining) in rat pons under the fourth ventricle at three different Bregma coordinates. Scale bar: 200 µm.*

B-G: *Representative images show control staining (no labeling without Satb1 primary antibody) and the localization of Satb1-positive SVTg neurons in rhesus macaque pontine sections (at Bregma -21.6 mm).* ***B-D*** *images show the map of pontine nuclei on coronal sections of one side of the dorsal pons. Scale bar: 500 µm.* ***E-G*** *images show SVTg areas (indicated with black boxes in* ***B-D****) at higher magnification. Scale bar: 50 µm. (****B*** *and* ***E****) Control staining without Satb1 primary antibody (****C*** *and* ***F****) Satb1 nuclear staining (black DAB-Ni precipitate) reveals a group of neurons (black arrowheads) under the fourth ventricle (4V). (****D*** *and* ***G****) ChAT cytosolic staining labels cholinergic neurons (black arrowheads) in the adjacent LDTg below SVTg in the monkey pons.*

H-O: *Representative images show control staining and the localization of Satb1-positive SVTg neurons in human pontine sections at two different coordinates.* ***H-K*** *images show the map of pontine nuclei on coronal sections of one side of the dorsal pons. Borders of SVTg are defined by*

the dense Satb1-positive neuronal labeling. Scale bar: 500 µm. ***L-O*** *images show a part of SVTg at higher magnification (indicated with black boxes in* ***H-K****). Scale bar: 50 µm.*

H, J, L, *and* ***N****: Control staining: images show no DAB-Ni labeling without the Satb1 primary antibody. The brown, natively lipofuscin or neuromelanin-expressing cells are detectable in LC and DR without staining.*

I, K, M, *and* ***O:*** *Satb1 nuclear staining (black DAB-Ni precipitate) reveals a group of neurons (black arrowheads) under the fourth ventricle (4V) in a human individual (SKO30). Abbreviations: 4V: fourth ventricle, DR: dorsal raphe, DTg: dorsal tegmentum, LC: locus coeruleus, LDTg: laterodorsal tegmentum, Me5: mesencephalic trigeminal nucleus, mlf: medial longitudinal fasciculus, PCG: pontine central grey, SVTg: subventricular tegmental nucleus. Published in (114).*

Table 5. Statistical details of behavioral experiments

Related figures	Experimental conditions	Groups	Mice	Medians	Interquartiles 25%	Interquartiles 75%	Statistical test and p values
Fig6B	Habituation 10min (HAB) (illum side % time)	CTRL	21	44,10%	32,60%	56,19%	Mann-Whitney U-tests: CTRL vs. ChR2: n.s.: p=0.088
		ChR2	19	52,84%	43,76%	59,03%	
	Real-time place preference 15min (RTPP) (illum side % time)	CTRL	21	52,52%	44,27%	68,72%	Mann-Whitney U-tests: CTRL vs. ChR2: ****: p=0.00003
		ChR2	19	18,86%	12,70%	36,64%	
	Conditioned place preference 5min (CPP) (illum side % time)	CTRL	21	55,98%	37,37%	80,27%	Mann-Whitney U-tests: CTRL vs. ChR2: *: p=0.045
		ChR2	19	28,50%	13,95%	54,11%	
Fig6D	Total number of nose pokes during base and stim	CTRL	11	39	23	46	Wilcoxon-test: base vs. stim: n.s.: p=0.722
				35	26	47	
	Total number of nose pokes during base and stim	ChR2	7	57	40	67	Wilcoxon-test: base vs. stim: *: p=0.018
				35	11	46	
Fig6E	Nose poke ration stim/base	CTRL	11	1,06	+/-0,47		Student's t-test: CTRL vs. ChR2: *: p=0.025; In case of these rows means and +/-SD are presented
		ChR2	7	0,56	+/-0,31		
Fig6F	ContextA 3min (CTXA) (freezing time %)	CTRL	13	13,68%	5,67%	17,57%	Mann-Whitney U-tests: CTXA CTRL vs. ArchT: *: p=0.025; gener CTRL vs. ArchT: *: p=0.026; cued CTRL vs. ArchT: *: p=0.011
		ArchT	9	3,00%	0,00%	6,11%	
	Generalized 3min (gener) (freezing time %)	CTRL	13	7,77%	1,11%	14,33%	
		ArchT	9	0,00%	0,00%	2,44%	
	Cued 1min (cued) (freezing time %)	CTRL	13	52,67%	43,33%	59,67%	
		ArchT	9	22,00%	21,33%	29,00%	
Fig8C	Habituation 10min (HAB) (illum side % time)	CTRL	17	42,65%	39,02%	48,75%	Mann-Whitney U-tests: CTRL vs. ChR2: n.s.: p=0.463
		ChR2	14	53,05%	37,15%	65,92%	
	Real-time place preference 10min (RTPP) (illum side % time)	CTRL	17	39,05%	34,40%	42,04%	Mann-Whitney U-tests: CTRL vs. ChR2: ****: p=0.00009
		ChR2	14	79,09%	59,66%	84,45%	
	Conditioned place preference 10min (CPP) (illum side % time)	CTRL	17	46,19%	32,98%	64,17%	Mann-Whitney U-tests: CTRL vs. ChR2: ***: p=0.0009
		ChR2	14	78,64%	63,90%	81,56%	

Fig8D	HAB	CTRL	17	42,65%	39,02%	48,75%	Wilcoxon-tests:
	RTPP			39,05%	34,40%	42,04%	HAB vs. RTPP: n.s.: p=0.653;
	CPP			46,19%	32,98%	64,17%	HAB vs. CPP: n.s.: p=0.407
	HAB	ChR2	14	53,05%	37,15%	65,92%	Wilcoxon-tests:
	RTPP			79,09%	59,66%	84,45%	HAB vs. RTPP: **: p=0.0015;
	CPP			78,64%	63,90%	81,56%	HAB vs. CPP: **: p=0.0012
Fig8F	Habituation 10min (HAB) (illum side % time)	CTRL	12	44,22%	38,92%	56,21%	Wilcoxon-tests: CTRL HAB vs. RTPP: n.s.: p=0.638; CTRL HAB vs. CPP: n.s.: p=0.937; ChR2 HAB vs. RTPP: *: p=0.015; ChR2 HAB vs. CPP: *: p=0.015
		ChR2	9	41,10%	33,36%	53,73%	
	Real-time place preference 10min (RTPP) (illum side % time)	CTRL	12	50,79%	37,79%	62,26%	
		ChR2	9	63,63%	48,88%	84,37%	
	Conditioned place preference 10min (CPP) (illum side % time)	CTRL	12	43,58%	29,34%	62,55%	
		ChR2	9	80,76%	47,31%	86,29%	
Fig8I	Illumulation side nosepokes (day 1)	CTRL	8	20	15,5	25,5	Mann-Whitney U-test:
		ChR2	8	35	28	38,5	CTRL vs. ChR2 day 1: *: p=0.031
	Illumulation side nosepokes (day 2)	CTRL	8	17	12	28	
		ChR2	8	31,5	18,5	50	CTRL vs. ChR2 day 2: n.s..: p=0.114
	Illumulation side nosepokes (day 3)	CTRL	8	18	14,5	26	
		ChR2	7	40	16	66	CTRL vs. ChR2 day 3: n.s..: p=0.103
	Illumulation side nosepokes (day 4)	CTRL	8	20	7,5	34	
		ChR2	8	39,5	20	64	CTRL vs. ChR2 day 4: m.n.s..: p=0.066
	Illumulation side nosepokes (day 5)	CTRL	8	13	10,5	27,5	
		ChR2	8	39,5	32,5	95	CTRL vs. ChR2 day 5: *: p=0.035
	Illumulation side nosepokes (day 6)	CTRL	8	32	14,5	48,5	
		ChR2	8	61	43,5	123	CTRL vs. ChR2 day 6: n.s..: p=0.128
	Illumulation side nosepokes (day 7)	CTRL	8	18	8,5	29,5	
		ChR2	8	64	39,5	84	CTRL vs. ChR2 day 7: *: p=0.014
	Illumulation side nosepokes (day 8)	CTRL	8	15	9,5	28,5	
		ChR2	8	34	18,5	52	CTRL vs. ChR2 day 8: *: p=0.040
	Illumulation side nosepokes (day 9)	CTRL	8	14	7,5	19	
		ChR2	8	33,5	18	76	CTRL vs. ChR2 day 9: *: p=0.024
	Illumulation side nosepokes (day 10)	CTRL	8	10	7	21,5	
		ChR2	8	82,5	47,5	108	CTRL vs. ChR2 day 10: **: p=0.0019
	Illumulation side nosepokes Extinction day (day 11)	CTRL	8	21,5	15	28	
		ChR2	8	41,5	25	59,5	CTRL vs. ChR2 day 11: *: p=0.021
Fig8J	Nosepoke number differences day11-day10 ILLUM side	CTRL	8	9,5	2	16	Mann-Whitney U-tests: illum side CTRL vs. ChR2: **: p=0.0023; NON side CTRL vs. ChR2: n.s.: p=0.461
		ChR2	8	-41	-57,5	-15,5	
	Nosepoke number differences day11-day10 NON side	CTRL	8	3	-1	10,5	
		ChR2	8	-0,5	-4,5	5	
Fig9C	Habituation 10min (HAB) (illum side % time)	CTRL	15	57,42%	44,39%	70,99%	Mann-Whitney U-test:
		stGtACR2	14	49,52%	44,93%	56,23%	CTRL vs. stGtACR2: n.s.: p=0.556
	Real-time place aversion 10min (RTPA) (illum side % time)	CTRL	15	60,67%	33,07%	66,47%	Mann-Whitney U-test:
		stGtACR2	14	24,25%	21,41%	30,44%	CTRL vs. stGtACR2: **: p=0.0016
	Conditioned place aversion 10min (CPA) (illum side % time)	CTRL	15	55,83%	36,96%	76,35%	Mann-Whitney U-test:
		stGtACR2	14	35,49%	25,34%	43,99%	CTRL vs. stGtACR2: *: p=0.015
Fig9D	HAB	CTRL	15	57,42%	44,39%	70,99%	Wilcoxon-tests:
	RTPA			60,67%	33,07%	66,47%	HAB vs. RTPA: n.s.: p=0.156;
	CPA			55,83%	36,96%	76,35%	HAB vs. CPA: n.s.: p=0.955
	HAB	stGtACR2	14	49,52%	44,93%	56,23%	Wilcoxon-tests:
	RTPA			24,25%	21,41%	30,44%	HAB vs. RTPA: ***: p=0.00098;
	CPA			35,49%	25,34%	43,99%	HAB vs. CPA: **: p=0.0052
Fig9F	1st shock 1min (freezing time %)	CTRL	15	0,00%	0,00%	0,00%	Mann-Whitney U-tests: 1st shock CTRL vs. stGtACR2: n.s.: p=0.715; 2nd shock CTRL vs. stGtACR2: n.s.: p=0.205; 3rd shock CTRL vs. stGtACR2: n.s.: p=0.983; 4th shock CTRL vs. stGtACR2: n.s.: p=0.256
		stGtACR2	14	0,00%	0,00%	0,00%	
	2nd shock 1min (freezing time %)	CTRL	15	0,00%	0,00%	4,58%	
		stGtACR2	14	4,66%	0,00%	7,57%	
	3rd shock 1min (freezing time %)	CTRL	15	11,00%	7,33%	16,56%	
		stGtACR2	14	10,13%	3,62%	22,33%	
	4th shock 1min (freezing time %)	CTRL	15	21,15%	8,54%	28,77%	
		stGtACR2	14	24,85%	18,00%	37,47%	
Fig9G	ContextA 5min (CTXA) (freezing time %)	CTRL	15	10,87%	5,45%	21,55%	Mann-Whitney U-tests: CTXA CTRL vs. stGtACR2: **: p=0.0064 CTXB CTRL vs. stGtACR2: **:p= 0.0015
		stGtACR2	14	26,32%	19,05%	42,78%	
	ContextB 5min (CTXB) (freezing time %)	CTRL	15	2,36%	0,00%	4,37%	
		stGtACR2	14	7,83%	4,82%	16,87%	

5. Discussion

5.1. Brainstem control of emotional balance

The brain processes emotional stimuli through a network of valence-encoding neural circuits, and the balance between these systems is essential for maintaining mental health (12,19). The mechanisms of emotional regulation are particularly significant in understanding psychiatric disorders like depression and anxiety, as these conditions often arise from dysfunctions in the brain's emotional processing systems (19,31,32,74). The LHb plays a central role in regulating emotional balance, and its dysfunction is closely linked to the development of depression (19,32,75,115). Previously, it was thought that LHb receive such information only from the forebrain (19,61,62,72,73). However, here we described two parallel pathways arising from the brainstem MRR vGluT2-positive and SVTg GABAergic neurons conveying aversive and reward-related information to the LHb, respectively (110,114). The identification and characterization of the surrounding pontine brainstem regions and their cell types, such as the serotonergic cells in the MRR and DR (87,116), cholinergic cells in the LDTg (117), and noradrenergic cells in the LC (116), were discovered early by using unique specific markers (TpH, ChAT, TH). However, identifying glutamatergic and GABAergic cells in the brainstem and mapping their connections has proven to be a much more challenging task. Cell-type-specific viral tract tracing techniques, combined with genetically modified mice enabled us to discover the MRR vGluT2-positive and the SVTg GABAergic neurons in the pontine brainstem.

5.2. The role of MRR vGluT2-positive neurons in processing negative experiences

LHb neurons are activated by negative or harmful events, which is essential for making appropriate decisions (15,29). Additionally, the septo-hippocampal system (MS/VDB-HIPP) is also activated, facilitating memory formation from such events (112,118,119). However, there was no known neuronal population in the brain that could simultaneously activate both of these systems, contributing to the immediate experience of a negative event and its rapid encoding as a memory. Although it has long been hypothesized that MRR neurons play a crucial role in the efficient processing of negative experiences and the formation of memory traces, their previously identified cell types, and their connections could not fully explain these functions (84,94,120). In our work,

we identified a previously unknown vGluT2-positive glutamatergic neuronal population in the MRR that constitutes 20% of the neurons in this region and gives the largest projecting cell population of the MRR. Anatomically, we found that MRR vGluT2-positive neurons innervate both the LHb and the HIPP-projecting MS/VDB neurons (Fig. 13), as well as other valence-processing-related subcortical regions. Additionally, we observed that MRR vGluT2-positive neurons receive synaptic inputs from several negative experience processing brain areas. Based on these anatomical findings, we proposed that MRR vGluT2-positive neurons are ideally positioned to mediate the rapid and efficient acquisition and encoding of negative experiences.

The LHb signals negative valence and negative reward-prediction errors by receiving rapid, immediate excitation during negative events or those expected to have a negative outcome (15,29,44,49,56,121). In vivo findings from my colleagues showed that MRR vGluT2-positive neurons are selectively and immediately activated by negative events (such as aversive airpuffs), but not activated by rewarding events (110). Our behavioral experiments revealed that activation of MRR vGluT2-positive neurons induced real-time and conditioned place avoidance, indicating that they encode negative valence and strongly suppressed motivation-driven behavior of mice. Furthermore, we found that the activation of MRR vGluT2-positive neurons during a negative experience is essential for the formation of a proper fear memory of an aversive event, whether context-based or associated with specific auditory cues. This likely occurs because, on the one hand, the activity of MRR vGluT2 neurons might be essential for the LHb during negative experiences. On the other hand, MS/VDB HIPP-projecting PV neurons cannot effectively initiate the hippocampal memory-forming network without the activity of MRR vGluT2-positive neurons. Therefore, we can conclude that MRR vGluT2-positive neurons serve a dual role during the acquisition of a negative experience: they activate the negative valence-encoding system, and they facilitate the rapid and efficient formation of a memory via the septo-hippocampal system (Fig. 13).

5.3. The role of SVTg neurons in processing positive experiences

The LHb is not only involved in processing negative experiences, but during rewarding events or those predicting a reward, LHb neurons are inhibited, encoding positive valence (56,60,63). Because the LHb has a negligible number of interneurons

(65), a critical question arises: how and from where does this reward-encoding inhibitory signal reach the LHb? Upon examining all GABAergic inhibitory inputs of the LHb, we discovered a previously unknown cell population in the pontine brainstem, which we named the SVTg based on its location. Using anatomical tract tracing, we demonstrated that the SVTg indeed provides GABAergic axonal terminals that innervated LHb neurons (Fig. 13), making SVTg the largest purely GABAergic input of the LHb. Further anatomical investigation revealed that the SVTg GABAergic neurons innervate not only the LHb, but several other valence-processing subcortical regions, as well as subcortical regions involved in memory formation (Fig. 13). We also found that SVTg GABAergic neurons receive synaptic inputs from brain areas that process salient environmental stimuli (PRN, mRT, Gi), negative experiences (MRR, IPN, LHb, LH), positive experiences (OFC, LDTg, DR, VTA) and decision-making (ACC, ZI, SC, SNr). The valence circuitry is evolutionarily ancient, with the LHb present across species from fishes to humans (12,18,19,22). Using the highly SVTg-specific Satb1 immunohistochemistry, we identified the SVTg neurons not only in mice but also in rat, monkeys, and humans, whereas previous studies reported Satb1-positive neurons under the fourth ventricle even in fishes (122). This suggests that the SVTg is evolutionarily highly conserved.

Fiber photometry findings of my colleagues showed that SVTg GABAergic neurons activated by both rewarding and reward-predicting stimuli conveying reward-related inhibitory signals to the LHb (114). Our behavioral experiments showed that stimulation of SVTg GABAergic neurons or their axonal fibers in the LHb induces both acute and conditioned place preference in mice, suggesting that SVTg activation encodes positive valence. Conversely, inhibition of SVTg neurons resulted in place avoidance behavior in mice. These findings imply that the baseline activity of the SVTg is essential for maintaining a normal motivational state during environmental exploration and during a direct rewarding experience, they encode positive valence by suppressing the activity of the LHb. Moreover, we also found that when given a choice, the mice self-stimulated their SVTg GABAergic neurons and continued to try compulsively, even after it became ineffective, suggesting that these cells may also contribute to reward-seeking and addictive behavior.

During a harmful, negative event, it is crucial that only a specific set of neurons encodes a negative experience to preserve scalability. At the behavioral level, this can prevent inappropriate fear responses or fear generalization. Over time, such processes could contribute to the development of disorders like anxiety or post-traumatic stress disorder (PTSD). Therefore, these systems may also require active inhibition during negative events. It is well known that a subset of LHb neurons are inhibited, rather than excited, by an aversive event (121,123). However, the source of this inhibition remains unknown. Fiber photometry findings of my colleagues revealed that SVTg GABAergic neurons also increase their activity during an aversive event, potentially mediating this partial inhibition in the LHb (114). Furthermore, our behavioral experiments demonstrated that inhibiting SVTg GABAergic neurons precisely during a negative experience significantly increased both contextual and generalized fear levels in mice. Thus, the SVTg GABAergic neurons not only inhibit the LHb during reward-related events, producing a positive experience, but also actively suppress the negative experience-encoding system of the brain during an aversive experience, preventing the network from over-activation.

5.4. Interactions between MRR vGluT2 and SVTg GABAergic neurons

Investigating the brainstem control of the LHb, we identified both an excitatory (MRR vGluT2) and an inhibitory (SVTg GABAergic) neuronal population in the pontine brainstem that project to the LHb (Fig. 13). Further examining their anatomical projections, we found that both MRR vGluT2-positive and SVTg GABAergic neurons project to similar brain regions, including valence-encoding subcortical brain areas, as well as memory-related brain regions (Fig. 13). Our observations showed that these two populations are also interconnected with each other. MRR vGluT2-positive neurons innervate the SVTg, and the SVTg project back to the MRR (Fig. 13). While MRR vGluT2-positive neurons primarily receive inputs from negative experience-processing systems and are likely under PFC cortical control; SVTg neurons receive more diverse inputs, including areas processing salience, positive and negative stimuli, and are under OFC cortical control (110,114). Our behavioral experiments showed that activation of MRR vGluT2-positive neurons induces negative experiences and reduces motivation, whereas, conversely, stimulation of SVTg neurons promotes reward-seeking behavior.

The activity of these two neuronal populations also differentially affects fear memory formation. We found that while the activation of MRR vGluT2-positive neurons is necessary for the formation of fear memories, the SVTg GABAergic neurons help to prevent over-activation of the negative valence-processing circuitry during fear acquisition. Thus, the activity of these two neuronal populations must remain in balance during various events to enable appropriate emotional evaluation, which is essential for guiding decision-making in the given moment. Therefore, a balanced activity between MRR vGluT2-positive and SVTg GABAergic neurons is required for the maintenance of emotional stability.

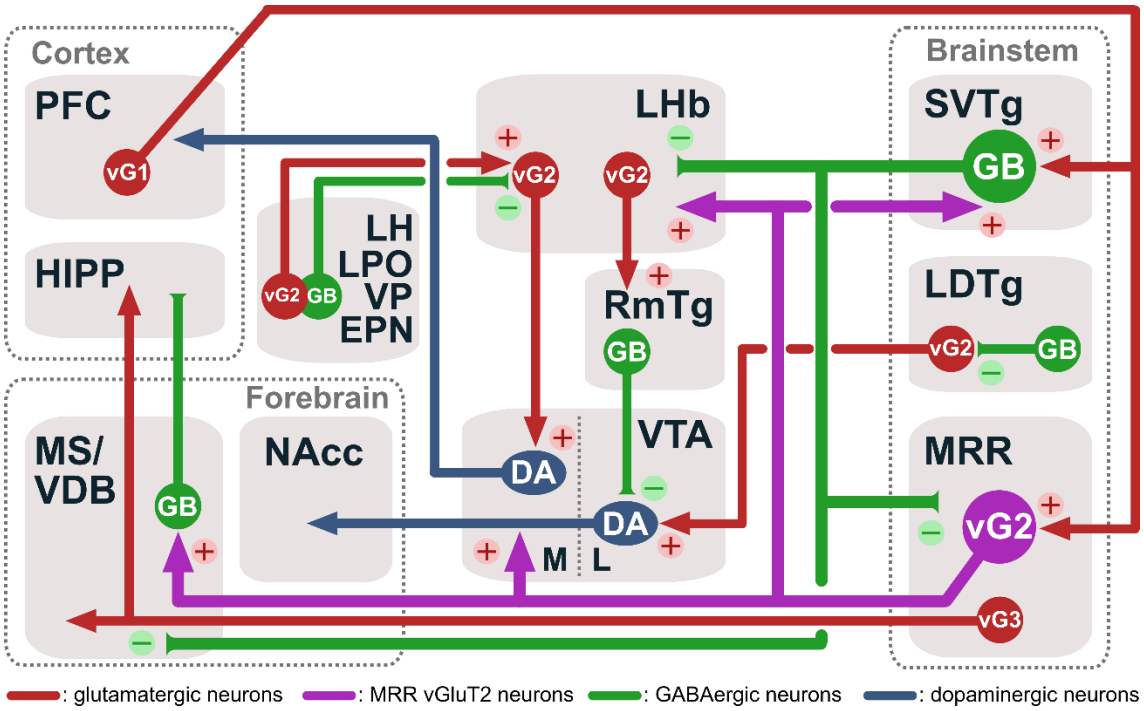

Figure 13. Summary of the anatomical connectivity of MRR vGluT2-positive and SVTg GABAergic neurons. *Schematic image shows that the brainstem can control the emotional valence and memory circuitries via its anatomical connections. Both the MRR vGluT2-positive and SVTg GABAergic neurons innervate the LHb, which coordinate emotional evaluation. Moreover, these two neuronal populations also innervate each other and other subcortical memory processing centers. Abbreviations: DA: dopaminergic neurons, GB: GABAergic neurons, vG1/vG2/vG3: vGluT1/vGluT2/vGluT3. (Own figure)*

5.5. Future therapeutic potential of MRR and SVTg

Hyperactivity of LHb neurons has been observed in depression, both in rodent models and in human individuals (19,32,77,79,124). In our studies, we demonstrated that the LHb receives inputs not only from the forebrain but is also significantly controlled by brainstem neurons. This brings up the important question of how these brainstem connections of the LHb might contribute to the development of psychiatric disorders such as depression. It can be reasonably hypothesized that the chronic hyperactivity of MRR vGluT2-positive neurons or the suppressed activity of SVTg GABAergic neurons could result in the hyperactivation of the LHb, which may contribute to the onset or the maintenance of depressive symptoms. Therefore, future therapeutic strategies targeting the inhibition of MRR vGluT2-positive neurons or the activation of SVTg GABAergic neurons may offer novel potential solutions for the treatment of depression. The early stages of Alzheimer's and Parkinson's diseases are known to be manifested in the pontine brainstem (125–127). Therefore, one may speculate that the MRR and SVTg may also contribute to the development of emotional dysfunction in these diseases due to the lack of optimal, balanced control of LHb neurons. Therefore, understanding the vulnerability of the MRR and SVTg neurons in these processes may help us better understand not only psychiatric disorders but also the side effects of neurodegenerative diseases in the future.

6. Conclusions

Despite significant advances in our understanding of brain function, the precise roles of several neurons and their pathways originating from subcortical regions remain largely unexplored. Further mapping of these regions and pathways will bring us closer to understanding how the brain operates as an integrated system, moving beyond localized functions to a more holistic understanding of neural interactions at the system level. Using multidisciplinary neuroscience tools from immunohistochemistry to optogenetic behavioral experiments, we found two previously unknown neuronal populations in the brainstem: the MRR vGluT2-positive and the SVTg GABAergic neurons. Our findings uncovered the functional neuroanatomy of these two neuronal populations and their crucial role in processing aversive and reward-related experiences, influencing behaviors such as fear memory formation and positive or negative valence assessment. As we deepen our knowledge of these specific valence-processing neural pathways, we move closer to a comprehensive model of how different brain regions, from the cortex and forebrain to the LHb and brainstem, interact to regulate complex emotional and cognitive functions. These insights are fundamental for building more accurate models of brain function, moving beyond the traditional focus on cortical areas to include the control of the brainstem in higher-order emotional processes. Additionally, pharmacologically targeting MRR vGluT2 or SVTg GABAergic neurons offers significant therapeutic potential for treating mood-related psychiatric disorders, such as depression and anxiety, where emotional dysregulation plays a central role. Therefore, this growing knowledge not only expands our understanding of the anatomical and functional architecture of the brain but also paves the way for innovative, more precise treatments with fewer side effects for diseases in neuropsychiatry.

7. Summary

Assigning appropriate emotional value to experiences and events is a key function of the LHb (19,29,44,115). This process is essential for decision-making and mood regulation, supporting our ability to adapt to the environment and ensuring survival (72,76). Forebrain inputs to the LHb could not fully explain its involvement in fast decision-making (19,64,115). Neuronal populations located in the brainstem appeared to be suitable to fulfill this role, though innervating the LHb, but these pathways remained completely unexplored. Here, we found two previously unrecognized neuronal populations in the brainstem that densely innervate the LHb. We described the anatomical connections of the brainstem MRR vGluT2-positive neurons, which send excitatory axonal collaterals to the LHb (110). Additionally, we identified a previously unknown GABAergic pontine brainstem nucleus, the SVTg, which, in contrast, sends inhibitory axons to the LHb (114). Our optogenetic behavior experiments revealed that stimulation of MRR vGluT2-positive neurons induced a negative, aversive experience, while stimulation of SVTg neurons induced a positive, reinforcing experience in mice. Moreover, we found that inhibition of MRR vGluT2-positive neurons during aversive experience suppressed, while, on the contrary, inhibition of SVTg neurons during aversive experience increased fear responses of mice. Both of these brainstem neurons receive inputs from several valence and salience-processing subcortical and cortical brain areas that can influence the activity of these cells. Our findings establish two key neuronal hubs in the pontine brainstem that oppositely regulate emotional valence and motivated behaviors in rodents, uncovering novel, fundamental brain mechanisms. These neurons may also play a central role in depression-related mood disorders and might potentially provide future therapeutic targets for these diseases.

8. References

1. Barrett, L. F., Lewis, M., & Haviland-Jones JM. Handbook of emotions. The Guilford Press. New York: The Guilford Press; 2018.
2. Laceulle OM, Ormel J, Vollebergh WAM, Aken MAG Van, Nederhof E. A test of the vulnerability model : temperament and temperament change as predictors of future mental disorders – the TRAILS study. J Child Psychol Psychiatry. 2014;3:227–36.
3. Malhi GS, Mann JJ. Depression. Lancet. 2018;392:2299–312.
4. Brody DJ, Pratt LA, Ph D, Hughes JP. Prevalence of Depression Among Adults Aged 20 and Over : Natl Cent Heal Stat. 2018;(303):2013–6.
5. Santomauro DF, Mantilla Herrera AM, Shadid J, Zheng P, Ashbaugh C, Pigott DM, Abbafati C, Adolph C, Amlag JO, Aravkin AY, Bang-Jensen BL, Bertolacci GJ, Bloom SS, Castellano R, Castro E, Chakrabarti S, Chattopadhyay J, Cogen RM, Collins JK, Dai X, Dangel WJ, Dapper C, Deen A, Erickson M, Ewald SB, Flaxman AD, Frostad JJ, Fullman N, Giles JR, Giref AZ, Guo G, He J, Helak M, Hulland EN, Idrisov B, Lindstrom A, Linebarger E, Lotufo PA, Lozano R, Magistro B, Malta DC, Månsson JC, Marinho F, Mokdad AH, Monasta L, Naik P, Nomura S, O'Halloran JK, Ostroff SM, Pasovic M, Penberthy L, Reiner RC, Reinke G, Ribeiro ALP, Sholokhov A, Sorensen RJD, Varavikova E, Vo AT, Walcott R, Watson S, Wiysonge CS, Zigler B, Hay SI, Vos T, Murray CJL, Whiteford HA, Ferrari AJ. Global prevalence and burden of depressive and anxiety disorders in 204 countries and territories in 2020 due to the COVID-19 pandemic. Lancet. 2021;398(10312):1700–12.
6. Chow W, Doane MJ, Sheehan J, Alphs L, Le H. Economic Burden Among Patients With Major Depressive Disorder: An Analysis of Healthcare Resource Use, Work Productivity, and Direct and Indirect Costs by Depression Severity. Am J Manag Care. 2019;
7. Bromet E, Andrade LH, Hwang I, Sampson NA, Alonso J, Girolamo G De, Graaf R De, Demyttenaere K, Hu C, Iwata N, Karam AN, Kaur J, Kostyuchenko S, Lépine J pierre, Levinson D, Matschinger H, Elena M, Mora M, Browne MO, Posada-villa J, Viana MC, Williams DR, Kessler RC. Cross-national epidemiology of DSM-IV major depressive episode. BMC Med. 2011;

8. Klonsky ED, May AM, Glenn CR. The Relationship Between Nonsuicidal Self-Injury and Attempted Suicide : Converging Evidence From Four Samples. J Abnorm Psychol. 2013;122(1):231–7.
9. Heim C, Binder EB. Current research trends in early life stress and depression : Review of human studies on sensitive periods , gene – environment interactions , and epigenetics. Exp Neurol. 2012;233(1):102–11.
10. Martin LA, Neighbors HW, Griffith DM. The experience of symptoms of depression in men vs women: Analysis of the national comorbidity survey replication. JAMA Psychiatry. 2013;70(10):1100–6.
11. Goldberg D, Fawcett J. The importance of anxiety in both major depression and bipolar disorder. Depress Anxiety. 2012;478:471–8.
12. Hu H. Reward and Aversion. Annu Rev Neurosci. 2016;297–314.
13. Schultz W. Dopamine signals for reward value and risk : basic and recent data. Behav Brain Funct. 2010;1–9.
14. Lammel S, Lim BK, Malenka RC. Reward and aversion in a heterogeneous midbrain dopamine system. Neuropharmacology. 2014;76 Pt B:351–9.
15. Matsumoto M, Hikosaka O. Representation of negative motivational value in the primate lateral habenula. Nat Neurosci. 2009;12(1):77–84.
16. Baker PM, Jhou T, Li B, Matsumoto M, Mizumori SJY, Stephenson-Jones M, Vicentic A. The Lateral Habenula Circuitry: Reward Processing and Cognitive Control. J Neurosci. 2016;36(45):11482–8.
17. Tovote P, Fadok JP, Lüthi A. Neuronal circuits for fear and anxiety. Nat Rev Neurosci. 2015;16(6):317–31.
18. Aizawa H, Amo R, Okamoto H. Phylogeny and ontogeny of the habenular structure. Front Neurosci. 2011;5(DEC):1–7.
19. Hu H, Cui Y, Yang Y. Circuits and functions of the lateral habenula in health and in disease. Nat Rev Neurosci. 2020;21(5):277–95.
20. Arsenault JT, Rima S, Stemmann H, Vanduffel W. Role of the primate ventral tegmental area in reinforcement and motivation. Curr Biol. 2014 Jun 16;24(12):1347–53.

21. Hennigan K, D'Ardenne K, McClure SM. Distinct midbrain and habenula pathways are involved in processing aversive events in humans. J Neurosci. 2015;35(1):198–208.
22. Stephenson-Jones M, Floros O, Robertson B, Grillner S. Evolutionary conservation of the habenular nuclei and their circuitry controlling the dopamine and 5-hydroxytryptophan (5-HT) systems. Proc Natl Acad Sci U S A. 2012;109(3).
23. Lammel S, Lim BK, Ran C, Huang KW, Betley MJ, Tye KM, Deisseroth K, Malenka RC. Input-specific control of reward and aversion in the ventral tegmental area. Nature. 2012;491(7423):212–7.
24. Pascoli V, Hiver A, Zessen R Van, Loureiro M, Achargui R, Harada M, Flakowski J, Lüscher C. Stochastic synaptic plasticity underlying compulsion in a model of addiction. Nature. 2018;564:366–71.
25. Coimbra B, Soares-Cunha C, Vasconcelos NAP, Domingues AV, Borges S, Sousa N, Rodrigues AJ. Role of laterodorsal tegmentum projections to nucleus accumbens in reward-related behaviors. Nat Commun. 2019;10(1):1–15.
26. Tovote P, Esposito MS, Botta P, Chaudun F, Fadok JP, Markovic M, Wolff SBE, Ramakrishnan C, Fenno L, Deisseroth K, Herry C, Arber S, Lüthi A, Jonathan P, Fadok JP, Markovic M, Wolff SBE, Ramakrishnan C, Fenno L, Deisseroth K, Herry C, Arber S, Lüthi A. Midbrain circuits for defensive behaviour. Nature. 2016;534(7606):206–12.
27. Wendt J, Weymar M, Lotze M, Hamm AO, Andreas L. Active avoidance and attentive freezing in the face of approaching threat. Neuroimage. 2017;158(June):196–204.
28. Jansen ASP, Van Nguyen X, Karpitskiy V, Mettenleiter TC, Loewy AD. Central command neurons of the sympathetic nervous system: Basis of the fight-or-flight response. Science. 1995;270(5236):644–6.
29. Matsumoto M, Hikosaka O. Lateral habenula as a source of negative reward signals in dopamine neurons. Nature. 2007;447(7148):1111–5.
30. Stopper CM, Tse MTL, Montes DR, Wiedman CR, Floresco SB. Overriding phasic dopamine signals redirects action selection during risk/reward decision making. Neuron. 2014;84(1):177–89.

31. Shin LM, Liberzon I. The Neurocircuitry of Fear , Stress , and Anxiety Disorders. Neuropsychopharmacology. 2009;35(1):169–91.
32. Yang Y, Cui Y, Sang K, Dong Y, Ni Z, Ma S, Hu H. Ketamine blocks bursting in the lateral habenula to rapidly relieve depression. Nature. 2018;554(7692):317–22.
33. Lawson RP, Nord CL, Seymour B, Thomas DL, Dayan P, Pilling S, Roiser JP. Disrupted habenula function in major depression. Mol Psychiatry. 2017 Feb 1;22(2):202–8.
34. Matsumoto M, Hikosaka O. Two types of dopamine neuron distinctly convey positive and negative motivational signals. Nature. 2009;459(7248):837–41.
35. Morales M, Margolis EB. Ventral tegmental area: cellular heterogeneity, connectivity and behaviour. Nat Rev Neurosci. 2017;
36. Coimbra B, Domingues AV, Soares-Cunha C, Correia R, Pinto L, Sousa N, Rodrigues AJ. Laterodorsal tegmentum–ventral tegmental area projections encode positive reinforcement signals. J Neurosci Res. 2021;99(11):3084–100.
37. Qi J, Zhang S, Wang HL, Wang H, De Jesus Aceves Buendia J, Hoffman AF, Lupica CR, Seal RP, Morales M. A glutamatergic reward input from the dorsal raphe to ventral tegmental area dopamine neurons. Nat Commun. 2014;5.
38. Jhou TC, Fields HL, Baxter MG, Saper CB, Holland PC. The rostromedial tegmental nucleus (RMTg), a GABAergic afferent to midbrain dopamine neurons, encodes aversive stimuli and inhibits motor responses. Neuron. 2009;61(5):786–800.
39. Berger B, Gaspar P, Verney C. Dopaminergic innervation of the cerebral cortex : unexpeded differences between rodents and primates. Science. 1991;(1966):35–9.
40. Root DH, Wang HL, Liu B, Barker DJ, Mód L, Szocsics P, Silva AC, Maglóczky Z, Morales M. Glutamate neurons are intermixed with midbrain dopamine neurons in nonhuman primates and humans. Sci Rep. 2016;6:30615.
41. Covey DP, Cheer JF. Accumbal Dopamine Release Tracks the Expectation of Dopamine Neuron-Mediated Reinforcement. Cell Rep. 2019;27(2):481-490.e3.
42. Tsai HC, Zhang F, Adamantidis A, Stuber GD, Bond A, De Lecea L, Deisseroth K. Phasic firing in dopaminergic neurons is sufficient for behavioral conditioning. Science. 2009 May 22;324(5930):1080–4.

43. Samson RD, Frank MJ, Fellous JM. Computational models of reinforcement learning: The role of dopamine as a reward signal. Cogn Neurodyn. 2010;4(2):91–105.
44. Bromberg-Martin ES, Hikosaka O. Lateral habenula neurons signal errors in the prediction of reward information. Nat Neurosci. 2011;14(9):1209–18.
45. Hong S, Jhou TC, Smith M, Saleem KS, Hikosaka O. Negative Reward Signals from the Lateral Habenula to Dopamine Neurons Are Mediated by Rostromedial Tegmental Nucleus in Primates. J Neurosci. 2011;31(32):11457–71.
46. Brinschwitz K, Dittgen A, Madai VI, Lommel R, Geisler S, Veh RW. Glutamatergic axons from the lateral habenula mainly terminate on GABAergic neurons of the ventral midbrain. Neuroscience. 2010;168(2):463–76.
47. de Jong JW, Afjei SA, Pollak Dorocic I, Peck JR, Liu C, Kim CK, Tian L, Deisseroth K, Lammel S. A Neural Circuit Mechanism for Encoding Aversive Stimuli in the Mesolimbic Dopamine System. Neuron. 2019;
48. Bromberg-Martin ES, Matsumoto M, Nakahara H, Hikosaka O. Multiple Timescales of Memory in Lateral Habenula and Dopamine Neurons. Neuron. 2010;67(3):499–510.
49. Bromberg-Martin ES, Matsumoto M, Hikosaka O. Distinct tonic and phasic anticipatory activity in lateral habenula and dopamine neurons. Neuron. 2010;67(1):144–55.
50. Gonzalez MC, Kramar CP, Tomaiuolo M, Katche C, Weisstaub N, Cammarota M, Medina JH. Medial prefrontal cortex dopamine controls the persistent storage of aversive memories. Front Behav Neurosci. 2014;8:408.
51. Rice MW, Roberts RC, Melendez-Ferro M, Perez-Costas E. Mapping dopaminergic deficiencies in the substantia nigra/ventral tegmental area in schizophrenia. Brain Struct Funct. 2016;221(1):185–201.
52. Grace AA. Dysregulation of the dopamine system in the pathophysiology of schizophrenia and depression. Nat Rev Neurosci. 2016;17(8):524–32.
53. Qin C, Luo M. Neurochemical phenotypes of the afferent and efferent projections of the mouse medial habenula. Neuroscience. 2009 Jul 7;161(3):827–37.

54. Klenowski PM, Zhao-Shea R, Freels TG, Molas S, Tapper AR. Dynamic activity of interpeduncular nucleus GABAergic neurons controls expression of nicotine withdrawal in male mice. Neuropsychopharmacology. 2022;47(3):641–51.
55. Wolfman SL, Gill DF, Bogdanic F, Long K, Al-Hasani R, McCall JG, Bruchas MR, McGehee DS. Nicotine aversion is mediated by GABAergic interpeduncular nucleus inputs to laterodorsal tegmentum. Nat Commun. 2018;9(1):1–11.
56. Wang D, Li Y, Feng Q, Guo Q, Zhou J, Luo M. Learning shapes the aversion and reward responses of lateral habenula neurons. Elife. 2017;6:1–20.
57. Golden SA, Heshmati M, Flanigan M, Christoffel DJ, Guise K, Pfau ML, Aleyasin H, Menard C, Zhang H, Hodes GE, Bregman D, Khibnik L, Tai J, Rebusi N, Krawitz B, Chaudhury D, Walsh JJ, Han MH, Shapiro ML, Russo SJ. Basal forebrain projections to the lateral habenula modulate aggression reward. Nature. 2016;534(7609):688–92.
58. Yang H, Yang J, Xi W, Hao S, Luo B, He X, Zhu L, Lou H, Yu Y qin, Xu F, Duan S, Wang H. Laterodorsal tegmentum interneuron subtypes oppositely regulate olfactory cue-induced innate fear. Nat Neurosci. 2016 Feb;19(2):283–9.
59. Stamatakis AM, Stuber GD. Activation of lateral habenula inputs to the ventral midbrain promotes behavioral avoidance. Nat Neurosci. 2012;15(8):1105–7.
60. Lalive AL, Congiu M, Lewis C, Groos D, Clerke JA, Tchenio A, Ge Y, Helmchen F, Mameli M. Synaptic inhibition in the lateral habenula shapes reward anticipation. Curr Biol. 2022;32(8):1829–36.
61. Barker DJ, Miranda-Barrientos J, Zhang S, Root DH, Wang HL, Liu B, Calipari ES, Morales M. Lateral Preoptic Control of the Lateral Habenula through Convergent Glutamate and GABA Transmission. Cell Rep. 2017;21(7):1757–69.
62. Zhang G wei, Shen L, Zhong W, Xiong Y, Zhang LI, Tao HW. Transforming Sensory Cues into Aversive Emotion via Septal-Habenular Pathway. Neuron. 2018;99(5):1016-1028.e5.
63. Shen L, Zhang GW, Tao C, Seo MB, Zhang NK, Huang JJ, Zhang LI, Tao HW. A bottom-up reward pathway mediated by somatostatin neurons in the medial septum complex underlying appetitive learning. Nat Commun. 2022;13(1):1–15.
64. Proulx CD, Hikosaka O, Malinow R. Reward processing by the lateral habenula in normal and depressive behaviors. Nat Neurosci. 2014;17(9):1146–52.

65. Webster JF, Vroman R, Sakata S, Wozny C. Disentangling neuronal inhibition and inhibitory pathways in the lateral habenula. 2019;44(0):1–52.
66. Liu X, Huang H, Zhang Y, Wang L, Wang F. Sexual Dimorphism of Inputs to the Lateral Habenula in Mice. Neurosci Bull. 2022;38(12):1439–56.
67. Meye FJ, Soiza-Reilly M, Smit T, Diana MA, Schwarz MK, Mameli M. Shifted pallidal co-release of GABA and glutamate in habenula drives cocaine withdrawal and relapse. Nat Neurosci. 2016;19(8):1019–24.
68. Root DH, Zhang S, Barker DJ, Miranda-Barrientos J, Liu B, Wang HL, Morales M. Selective Brain Distribution and Distinctive Synaptic Architecture of Dual Glutamatergic-GABAergic Neurons. Cell Rep. 2018;23(12):3465–79.
69. Quina LA, Tempest L, Ng L, Harris JA, Ferguson S, Jhou TC, Turner EE. Efferent pathways of the mouse lateral habenula. J Comp Neurol. 2015;523(1):32–60.
70. Laurent V, Wong FL, Balleine BW. The Lateral Habenula and Its Input to the Rostromedial Tegmental Nucleus Mediates Outcome-Specific Conditioned Inhibition. J Neurosci. 2017;37(45):10932–42.
71. Knowland D, Lilascharoen V, Pacia CP, Shin S, Wang EHJ, Lim BK. Distinct Ventral Pallidal Neural Populations Mediate Separate Symptoms of Depression. Cell. 2017;
72. Stephenson-Jones M, Yu K, Ahrens S, Tucciarone JM, Van Huijstee AN, Mejia LA, Penzo MA, Tai LH, Wilbrecht L, Li B. A basal ganglia circuit for evaluating action outcomes. Nature. 2016;539(7628):289–93.
73. Lazaridis I, Tzortzi O, Weglage M, Märtin A, Xuan Y, Parent M, Johansson Y, Fuzik J, Fürth D, Fenno LE, Ramakrishnan C, Silberberg G, Deisseroth K, Carlén M, Meletis K. A hypothalamus-habenula circuit controls aversion. Mol Psychiatry. 2019;24:1351–1368.
74. Shabel SJ, Wang C, Monk B, Aronson S, Malinow R. Stress transforms lateral habenula reward responses into punishment signals. Proc Natl Acad Sci U S A. 2019 Jun 18;116(25):12488–93.
75. Li K, Zhou T, Liao L, Yang Z, Wong C, Henn F, Malinow R, Yates JR, Hu H. βCaMKII in lateral habenula mediates core symptoms of depression. Science. 2013;341(6149):1016–20.

76. Hikosaka O. The habenula: from stress evasion to value-based decision-making. Nat Rev Neurosci. 2010 Jul;11(7):503–13.
77. Aizawa H, Cui W, Tanaka K, Okamoto H. Hyperactivation of the habenula as a link between depression and sleep disturbance. Front Hum Neurosci. 2013;7(December):1–6.
78. Li B, Piriz J, Mirrione M, Chung C, Proulx CD, Schulz D, Henn F, Malinow R. Synaptic potentiation onto habenula neurons in the learned helplessness model of depression. Nature. 2011;470(7335):535–9.
79. Cui Y, Yang Y, Ni Z, Dong Y, Cai G, Foncelle A, Ma S, Sang K, Tang S, Li Y, Shen Y, Berry H, Wu S, Hu H. Astroglial Kir4.1 in the lateral habenula drives neuronal bursts in depression. Nature. 2018;554(7692):323–7.
80. Zhang H, Li K, Chen HS, Gao SQ, Xia ZX, Zhang JT, Wang F, Chen JG. Dorsal raphe projection inhibits the excitatory inputs on lateral habenula and alleviates depressive behaviors in rats. Brain Struct Funct. 2018;223(5):2243–58.
81. Sartorius A, Kiening KL, Kirsch P, von Gall CC, Haberkorn U, Unterberg AW, Henn FA, Meyer-Lindenberg A. Remission of Major Depression Under Deep Brain Stimulation of the Lateral Habenula in a Therapy-Refractory Patient. Biol Psychiatry. 2010;67(2):e9–11.
82. Zhang C, Kim SG, Li D, Zhang Y, Li Y, Husch A, Hertel F, Yan F, Voon V, Sun B. Habenula deep brain stimulation for refractory bipolar disorder. Brain Stimul. 2019;12(5):1298–300.
83. Venkatraman A, Edlow BL, Immordino-Yang MH. The brainstem in emotion: A review. Front Neuroanat. 2017;11(March):1–12.
84. Varga V, Losonczy A, Zemelman B V., Borhegyi Z, Nyiri G, Domonkos A, Hangya B, Holderith N, Magee JC, Freund TF. Fast synaptic subcortical control of hippocampal circuits. Science. 2009;326(5951):449–53.
85. Szőnyi A, Mayer MI, Cserép C, Takács VT, Watanabe M, Freund TF, Nyiri G. The ascending median raphe projections are mainly glutamatergic in the mouse forebrain. Brain Struct Funct. 2016;221(2):735–51.

86. Szőnyi A, Sos KE, Nyilas R, Schlingloff D, Domonkos A, Takács VT, Pósfai B, Hegedüs P, Priestley JB, Gundlach AL, Gulyás AI, Varga V, Losonczy A, Freund TF, Nyiri G. Brainstem nucleus incertus controls contextual memory formation. Science. 2019;364(6442):0–14.
87. Hensler JG. Serotonergic modulation of the limbic system. 2006;30:203–14.
88. Moncrieff J, Cooper RE, Stockmann T, Amendola S, Hengartner MP, Horowitz MA. The serotonin theory of depression: a systematic umbrella review of the evidence. Mol Psychiatry. 2023;28(8):3243–56.
89. Balázsfi DG, Zelena D, Farkas L, Demeter K, Barna I, Cserép C, Takács VT, Nyíri G, Gölöncsér F, Sperlágh B, Freund TF, Haller J. Median raphe region stimulation alone generates remote, but not recent fear memory traces. PLoS One. 2017;12(7):e0181264.
90. Beliveau V, Svarer C, Frokjaer VG, Knudsen GM, Greve DN, Fisher PM. Functional connectivity of the dorsal and median raphe nuclei at rest. Neuroimage. 2015 Aug 1;116:187–95.
91. Ren J, Friedmann D, Xiong J, Liu CD, Ferguson BR, Weerakkody T, DeLoach KE, Ran C, Pun A, Sun Y, Weissbourd B, Neve RL, Huguenard J, Horowitz MA, Luo L. Anatomically Defined and Functionally Distinct Dorsal Raphe Serotonin Sub-systems. Cell. 2018;175(2):472-487.e20.
92. Commons KG. Dorsal raphe organization. J Chem Neuroanat. 2020;110(October):101868.
93. Nakamura K. The role of the dorsal raphé nucleus in reward-seeking behavior. Front Integr Neurosci. 2013;7(AUG):1–18.
94. Sos KE, Mayer MI, Cserép C, Takács FS, Szőnyi A, Freund TF, Nyiri G. Cellular architecture and transmitter phenotypes of neurons of the mouse median raphe region. Brain Struct Funct. 2017;222(1):287–99.
95. Vertes RP, Fortin WJ, Crane AM. Projections of the median raphe nucleus in the rat. J Comp Neurol. 1999;
96. Breton-Provencher V, Drummond GT, Sur M. Locus Coeruleus Norepinephrine in Learned Behavior: Anatomical Modularity and Spatiotemporal Integration in Targets. Front Neural Circuits. 2021;15(June):1–11.

97. Morris LS, McCall JG, Charney DS, Murrough JW. The role of the locus coeruleus in the generation of pathological anxiety. Brain Neurosci Adv. 2020;4:239821282093032.

98. Liu C, Tose AJ, Verharen JPH, Zhu Y, Tang LW, de Jong JW, Du JX, Beier KT, Lammel S. An inhibitory brainstem input to dopamine neurons encodes nicotine aversion. Neuron. 2022;110(18):3018-3035.e7.

99. Du Y, Zhou S, Ma C, Chen H, Du A, Deng G, Liu Y, Tose AJ, Sun L, Liu Y, Wu H, Lou H, Yu Y qin, Zhao T, Lammel S, Duan S, Yang H. Dopamine release and negative valence gated by inhibitory neurons in the laterodorsal tegmental nucleus. Neuron. 2023;111(19):3102-3118.e7.

100. Fischer NM, Hinkle JT, Perepezko K, Bakker CC, Morris M, Broen MPG, Butala A, Dawson TM, Leentjens AFG, Mari Z, Marvel CL, Mills KA, Rosenthal LS, Shepard MD, Pantelyat A, Bakker A, Pletnikova O, Troncoso JC, Wang J, Pontone GM. Brainstem Pathologies Correlate With Depression and Psychosis in Parkinson's Disease. Am J Geriatr Psychiatry. 2021;29(9):958–68.

101. Elvsåshagen T, Bahrami S, van der Meer D, Agartz I, Alnæs D, Barch DM, Baur-Streubel R, Bertolino A, Beyer MK, Blasi G, Borgwardt S, Boye B, Buitelaar J, Bøen E, Celius EG, Cervenka S, Conzelmann A, Coynel D, Di Carlo P, Djurovic S, Eisenacher S, Espeseth T, Fatouros-Bergman H, Flyckt L, Franke B, Frei O, Gelao B, Harbo HF, Hartman CA, Håberg A, Heslenfeld D, Hoekstra PJ, Høgestøl EA, Jonassen R, Jönsson EG, Farde L, Flyckt L, Engberg G, Erhardt S S, Fatouros-Bergman H, Cervenka S, Schwieler L, Piehl F, Agartz I, Collste K, Victorsson P, Malmqvist A, Hedberg M, Orhan F, Sellgren CM, Kirsch P, Kłoszewska I, Lagerberg TV, Landrø NI, Le Hellard S, Lesch KP, Maglanoc LA, Malt UF, Mecocci P, Melle I, Meyer-Lindenberg A, Moberget T, Nordvik JE, Nyberg L, Connell KSO, Oosterlaan J, Papalino M, Papassotiropoulos A, Pauli P, Pergola G, Persson K, de Quervain D, Reif A, Rokicki J, van Rooij D, Shadrin AA, Schmidt A, Schwarz E, Selbæk G, Soininen H, Sowa P, Steen VM, Tsolaki M, Vellas B, Wang L, Westman E, Ziegler GC, Zink M, Andreassen OA, Westlye LT, Kaufmann T. The genetic architecture of human brainstem structures and their involvement in common brain disorders. Nat Commun. 2020;11(1).

102. Kim M, Kwak S, Yoon YB, Kwak Y Bin, Kim T, Cho KIK, Lee TY, Kwon JS. Functional connectivity of the raphe nucleus as a predictor of the response to selective serotonin reuptake inhibitors in obsessive-compulsive disorder. Neuropsychopharmacology. 2019;44(12):2073–81.
103. Szabadits E, Cserép C, Ludányi A, Katona I, Gracia-Llanes J, Freund TF, Nyíri G. Hippocampal GABAergic synapses possess the molecular machinery for retrograde nitric oxide signaling. J Neurosci. 2007;27(30):8101–11.
104. Rovó Z, Ulbert I, Acsády L. Drivers of the primate thalamus. J Neurosci Off J Soc Neurosci. 2012 Dec;32(49):17894–908.
105. Wickersham IR, Lyon DC, Barnard RJO, Mori T, Finke S, Conzelmann KK, Young JAT, Callaway EM. Monosynaptic restriction of transsynaptic tracing from single, genetically targeted neurons. Neuron [Internet]. 2007;53(5):639–47. Available from: http://www.ncbi.nlm.nih.gov/pubmed/17329205%0Ahttp://www.pubmedcentral.nih.gov/articlerender.fcgi?artid=PMC2629495
106. Kim EJ, Jacobs MW, Ito-Cole T, Callaway EM. Improved Monosynaptic Neural Circuit Tracing Using Engineered Rabies Virus Glycoproteins. Cell Rep. 2016;15(4):692–9.
107. Sterio DC. The unbiased estimation of number and sizes of arbitrary particles using the disector. J Microsc. 1984 May;134(Pt 2):127–36.
108. Schmitz C, Hof PR. Design-based stereology in neuroscience. Neuroscience. 2005;130(4):813–31.
109. West MJ, Slomianka L, Gundersen HJG. Unbiased stereological estimation of the total number of neurons in the subdivisions of the rat hippocampus using the optical fractionator. Anat Rec. 1991;
110. **Szőnyi A, Zichó K, Barth AM, Gönczi RT, Schlingloff D, Török B, Sipos E, Major A, Bardóczi Z, Sos KE, Gulyás AI, Varga V, Zelena D, Freund TF, Nyiri G. Median raphe controls acquisition of negative experience in the mouse. Science. 2019;366(6469):eaay8746.**
111. Buzsáki G, Moser EI. Memory, navigation and theta rhythm in the hippocampal-entorhinal system. Nat Neurosci. 2013;16(2):130–8.

112. Hangya B, Borhegyi Z, Szilagyi N, Freund TF, Varga V. GABAergic Neurons of the Medial Septum Lead the Hippocampal Network during Theta Activity. J Neurosci. 2009;29(25):8094–102.

113. Borhegyi Z, Varga V, Szilágyi N, Fabo D, Freund TF. Phase segregation of medial septal GABAergic neurons during hippocampal theta activity. J Neurosci. 2004;24(39):8470–9.

114. **Zichó K, Balog BZ, Sebestény RZ, Brunner J, Takács V, Barth AM, Seng C, Orosz Á, Manó A, Sebők H, Mikics E, Földy C, Szabadics J, Nyiri G. Identification of the subventricular tegmental nucleus as brainstem reward center. Science. 2025;2191(Vol 387, Issue 6732).**

115. Groos D, Helmchen F. The lateral habenula: A hub for value-guided behavior. Cell Rep. 2024;43(4):113968.

116. Felten DL, Sladek JR. Monoamine distribution in primate brain V. Monoaminergic nuclei: Anatomy, pathways and local organization. Brain Res Bull. 1983;10(2):171–284.

117. Satoh K, Fibiger HC. Cholinergic neurons of the laterodorsal tegmental nucleus: Efferent and afferent connections. J Comp Neurol. 1986;253(3):277–302.

118. Colom L V. Septal networks: relevance to theta rhythm, epilepsy and Alzheimer's disease. J Neurochem. 2006 Feb;96(3):609–23.

119. Gangadharan G, Shin J, Kim SW, Kim A, Paydar A, Kim DS, Miyazaki T, Watanabe M, Yanagawa Y, Kim J, Kim YS, Kim D, Shin HS. Medial septal GABAergic projection neurons promote object exploration behavior and type 2 theta rhythm. Proc Natl Acad Sci. 2016;113(23):6550–5.

120. Vertes RP, Kocsis B, Vertes, R P and Kocsis B. Brainstem-diencephalo-septohippocampal systems controlling the theta rhythm of the hippocampus. Neuroscience. 1997;81(4):893–926.

121. Congiu M, Trusel M, Pistis M, Mameli M, Lecca S. Opposite responses to aversive stimuli in lateral habenula neurons. Eur J Neurosci. 2019;50(6):2921–30.

122. Lozano D, López JM, Jiménez S, Morona R, Ruíz V, Martínez A, Moreno N. Expression of SATB1 and SATB2 in the brain of bony fishes: what fish reveal about evolution. Brain Struct Funct. 2023;228(3–4):921–45.

123. Congiu M, Mondoloni S, Zouridis IS, Schmors L, Lecca S, Lalive AL, Ginggen K, Deng F, Berens P, Paolicelli RC, Li Y, Burgalossi A, Mameli M. Plasticity of neuronal dynamics in the lateral habenula for cue-punishment associative learning. Mol Psychiatry. 2023;(January).
124. Ranft K, Dobrowolny H, Krell D, Bielau H, Bogerts B, Bernstein HG. Evidence for structural abnormalities of the human habenular complex in affective disorders but not in schizophrenia. Psychol Med. 2010;40(4):557–67.
125. Simic G, Stanic G, Mladinov M, Jovanov-Milosevic N, Kostovic I, Hof PR. Does Alzheimer's disease begin in the brainstem?: Annotation. Neuropathol Appl Neurobiol. 2009;35(6):532–54.
126. Lee JH, Ryan J, Andreescu C, Aizenstein H, Lim HK. Brainstem morphological changes in Alzheimer's disease. Neuroreport. 2015;26(7):411–5.
127. Braak H, Ghebremedhin E, Rüb U, Bratzke H, Del Tredici K. Stages in the development of Parkinson's disease-related pathology. Cell Tissue Res. 2004;318(1):121–34.

9. Bibliography of the candidate's publications

Original publications related to the PhD thesis:

Zichó K, Balog BZ, Sebestény RZ, Brunner J, Takács V, Barth AM, Seng C, Orosz Á, Aliczki M, Sebők H, Mikics E, Földy C, Szabadics J, Nyiri G.
Identification of the subventricular tegmental nucleus as brainstem reward center.
SCIENCE
2025 Jan 24;387:eadr2191. doi: 10.1126/science.adr2191. PMID: 39847621
IF: 44.7

Szőnyi A*, **Zichó K*,** Barth AM, Gönczi RT, Schlingloff D, Török B, Sipos E, Major A, Bardóczi Z, Sos KE, Gulyás AI, Varga V, Zelena D, Freund TF, Nyiri G.
Median raphe controls acquisition of negative experience in the mouse.
SCIENCE
2019 Nov 29;366(6469):eaay8746. doi: 10.1126/science.aay8746. PMID: 31780530.
*: contributed equally
IF: 41.846

Original publications not related to the PhD thesis:

Zichó K, Sos KE, Papp P, Barth AM, Misák E, Orosz Á, Mayer MI, Sebestény RZ, Nyiri G.
Fear memory recall involves hippocampal somatostatin interneurons.
PLOS BIOLOGY
2023 Jun 8;21(6):e3002154. doi: 10.1371/journal.pbio.3002154. PMID: 37289847; PMCID: PMC10284381.
IF: 7.8

Takacs V, Papp P, Orosz Á, Bardóczi Z, Zsoldos T, **Zichó K**, Watanabe M, Maglóczky Z, Gombás P, Freund TF, Nyiri G.

Absolute number of three populations of interneurons and all GABAergic synapses in the human hippocampus.

THE JOURNAL OF NEUROSCIENCE

2025 March 5:e0372242024. doi: 10.1523/JNEUROSCI.0372-24.2024. PMID: 39809540.

IF: 4.4

10. Acknowledgements

I would like to express my gratitude to my supervisor, Dr. Gábor Nyiri, whose expertise and dedication have guided and supported my research career for more than eight years. I am deeply thankful to all the current members of the Cortical Research Group at the HUN-REN Institute of Experimental Medicine, especially to Boldizsár Balog, Réka Sebestény, Virág Takács, Zsuzsanna Bardóczi, Albert Barth, Áron Orosz, Hunor Sebők, and Erik Misák, who helped my research. I would like to thank former group members, including András Szőnyi, Katalin Sós, Péter Papp, and Márton Mayer, for their guidance in teaching me essential methods and fostering scientific critical thinking. Additionally, I am thankful to our group's assistants, Emőke Szépné Simon, Nándor Kriczky, and Katalin Iványi, for their contributions to the smooth conduct of the experiments. Furthermore, I am grateful to our collaborators, both within and beyond the institute, whose contributions complemented our work and enhanced our discoveries. I am also thankful for the financial support of the project provided by the New National Excellence Program by the Ministry of Innovation (ÚNKP-20-3-I-SE-31, ÚNKP-21-3-SE-9, ÚNKP-22-3-II-SE-7, ÚNKP-23-3-II-SE-24), the Semmelweis 250+ Excellence PhD Fellowship (EFOP-3.6.3-VEKOP-16-2017-00009), the Stephen W. Kuffler PhD Scholarship, and the Gedeon Richter Talentum Foundation within the framework of the Gedeon Richter Excellence PhD Scholarship. Finally, I would like to express my heartfelt gratitude to my wife, Andrea Kásler, for her unwavering support through my successes and challenges over the past six years. I am also deeply thankful to my parents and my friends for their steadfast encouragement in my everyday life.